DOI 10.59887/2073-6673.2024.17(4)-1

UDC 551.468

© *V. V. Zhmur*[1–3], *T. V. Belonenko*[1]*, *E. V. Novoselova*[1,4], *B. P. Suetin*[3], 2024

[1]St. Petersburg State University, 7–9 Universitetskaya Emb., St. Petersburg, 199034, Russia
[2]Shirshov Institute of Oceanology, Russian Academy of Sciences, 36 Nakhimovsky Prosp., Moscow, 117997, Russia
[3]Moscow Institute of Physics and Technology (National Research University), 9 Institutskiy per., Dolgoprudny, Moscow Region, 141701, Russia
[4]Nansen International Environmental and Remote Sensing Center Scientific Foundation, 7 Line 14 V.O., St. Petersburg, 199034, Russia
*btvlisab@yandex.ru

EVOLUTION OF MESOSCALE VORTICES IN THE OCEAN INTO FILAMENTS INFERRED FROM ALTIMETER DATA

Received 27.08.2024, Revised 11.11.2024, Accepted 27.11.2024

Abstract

Satellite remote sensing techniques offer a wealth of optical, infrared (IR), and radar images of the ocean surface, where we can observe numerous elongated vortex structures known as filaments. These filaments become readily visible in the imagery due to the presence of surfactant films and/or floating algae clusters on the sea's surface. Given their elongated form, automated vortex identification methods do not readily distinguish filaments from vortices. Nevertheless, both filaments and vortices exhibit notable characteristics such as high relative vorticity and kinetic energy. The process by which vortices transform into filaments is a result of their interaction with spatially non-uniform background currents. In this study, we apply the theoretical principles regarding the stretching of mesoscale ocean vortices to real ocean conditions, inferred from altimeter data. The primary objective of this research is to assess the proportion of mesoscale ocean vortices that undergo stretching to become filaments, consequently facilitating the redistribution of energy from the mesoscale to the submesoscale. We provide a total assessment of the portion of the World Ocean's surface where mesoscale vortices undergo significant stretching. We present maps that indicate the geographical distribution of regions where vortex stretching is not restricted and offer an interpretation of the findings. The reduction in the inherent energy of vortices due to the stretching induced by the background flow is explained as a potential mechanism for energy transfer from the vortex to the flow, possibly leading to the manifestation of the negative viscosity effect within this system.

Keywords: mesoscale vortices, filaments, elongation, ellipsoid, energy, negative viscosity

УДК 551.468

© *В. В. Жмур*[1–3], *Т. В. Белоненко*[1]*, *Е. В. Новоселова*[1,4], *Б. П. Суетин*[3], 2024

[1]Санкт-Петербургский государственный университет, 199034, Университетская наб., д. 7–9, г. Санкт-Петербург
[2]Институт океанологии им. П.П. Ширшова РАН, 117997, Нахимовский проспект, д. 36, г. Москва
[3]Московский физико-технический институт (национальный исследовательский университет), 141701, Институтский пер., 9, г. Долгопрудный, Московская область
[4]Научный фонд «Международный центр по окружающей среде и дистанционному зондированию имени Нансена», 199034, 14 линия В.О., д. 7, г. Санкт-Петербург
*btvlisab@yandex.ru

ТРАНСФОРМАЦИЯ МЕЗОМАСШТАБНЫХ ОКЕАНИЧЕСКИХ ВИХРЕЙ В ФИЛАМЕНТЫ: АНАЛИЗ ДАННЫХ АЛЬТИМЕТРИИ

Статья поступила в редакцию 27.08.2024, после доработки 11.11.2024, принята в печать 27.11.2024

Аннотация

Спутниковые данные дистанционного зондирования предоставляют обширный массив оптических, инфракрасных (ИК) и радиолокационных изображений поверхности океана, на которых видны многочисленные вытянутые вихревые структуры — филаменты. Их высокая контрастность на изображениях обусловлена наличием поверхностно-активных пленок и/или скоплений водорослей. Из-за вытянутой формы филаменты трудно отличить от вихрей с помощью автома-

Ссылка для цитирования: *Жмур В.В.*, *Белоненко Т.В.*, *Новоселова Е.В.*, *Суетин Б.П.* Трансформация мезомасштабных океанических вихрей в филаменты: анализ данных альтиметрии // Фундаментальная и прикладная гидрофизика. 2024. Т. 17, № 4. 8–31. doi: 10.59887/2073-6673.2024.17(4)-1
For citation: Zhmur V.V., Belonenko T.V., Novoselova E.V., Suetin B.P. Evolution of Mesoscale Vortices in the Ocean into Filaments Inferred from Altimeter Data. *Fundamental and Applied Hydrophysics.* 2024;17(4):8–31. doi: 10.59887/2073-6673.2024.17(4)-1

тизированных методов идентификации. Однако и филаменты, и вихри характеризуются высокой относительной завихренностью и кинетической энергией. Трансформация вихрей в филаменты обусловлена взаимодействием с неоднородными фоновыми течениями. В данном исследовании применяется теоретическая модель растяжения мезомасштабных океанических вихрей к реальным данным альтиметрии. Цель исследования — оценить долю мезомасштабных вихрей, претерпевающих растяжение и трансформирующихся в филаменты, что приводит к перераспределению энергии с мезомасштаба на субмезомасштаб. Оценивается глобальное пространственное распределение областей с неограниченным и ограниченным растяжением мезомасштабных вихрей и интерпретируются полученные результаты. Уменьшение энергии вихрей за счет растяжения, вызванного фоновым потоком, рассматривается как потенциальный механизм передачи энергии от вихря к потоку, что может проявляться в виде эффекта отрицательной вязкости.

Ключевые слова: мезомасштабные вихри, филаменты, вытягивание, эллипсоид, энергия, отрицательная вязкость

1. Introduction

Mesoscale eddies play a vital role in horizontal and vertical water exchange, influence the spatial distribution of oceanographic parameters, and have a substantial impact on bioproductivity [1]. The existence of ocean eddies, such as those found in the Gulf Stream or Kuroshio, has been known to humanity for an extended period. However, advancements in measurement technology have enabled both direct and indirect assessments of these formations in the World Ocean only since the latter half of the 20th century. This progress occurred with the involvement of specialized research vessels equipped for the study of these phenomena. The true surge in the exploration of mesoscale eddies began following scientific ocean experiments such as POLYGON-70 in the North Atlantic, MODE (Sargasso Sea, 1973), POLYMODE (North Atlantic, 1977–1978), MESOPOLYGON (North Atlantic, 1985), and MEGAPOLIGON (Pacific Ocean, 1987). These expeditions sparked widespread interest in the global scientific community for both experimental and theoretical investigations of oceanic vortex formations with horizontal dimensions ranging from a few tens of kilometers to 100–200 km.

Mesoscale eddies within the ocean play a pivotal role in transferring the energy of water movement and in shaping the variability of hydrophysical and hydrochemical fields across the ocean's scale spectrum [2]. With the discovery of mesoscale eddies, the prior concept of the ocean as a relatively stable entity in space and time gave way to a new understanding. According to this perspective, the primary energy of sea water movement is concentrated within eddies, rather than in the average circulation of the ocean.

Criteria and detection algorithms have been developed for eddies, which are considered closed formations. The rapid advancement of remote sensing techniques, especially altimetry products, along with the increased computational capabilities, has spurred the rapid development of automated algorithms for detecting and tracking eddies. The significance of these algorithms lies in their ability to shift from analyzing the areal characteristics of vortex processes, such as vortex kinetic energy, to examining specific vortex parameters like radius, amplitude, orbital velocity, lifetime, and movement velocity.

Despite their diverse approaches, automated eddy identification and tracking methods can be categorized into three general groups: physical, geometric, and hybrid [3]. In physical methods, criteria are directly derived from the values of the initial field. Geometric methods, on the other hand, focus exclusively on the geometric characteristics of isolines in the initial parameter when selecting vortices. Mixed algorithms, as the name suggests, differentiate vortices based on both the physical values and geometric characteristics of the initial field.

However, the ability of all these methods to distinguish filaments within oceanographic fields is constrained, primarily by the spatial resolution of the data, and secondly, algorithmically, as these algorithms typically don't differentiate elongated structures like filaments. This may explain the relatively lower interest of oceanographers in filaments compared to eddies.

Filaments become discernible in optical, infrared, and radar images of the ocean surface owing to the presence of surfactant films and/or floating algae on the sea surface (please refer to Fig. 1 for ocean filaments). Temperature anomalies in filaments often serve as crucial mechanisms for generating light/dark patterns in radar images [4]. One of the mechanisms contributing to filament formation is the transformation of vortices through stretching under the influence of spatially non-uniform background flows when one of the horizontal scales becomes several times larger than the other. For instance, this transformation of a vortex is illustrated in [5]. In their study, the authors analyzed the evolution of a mesoscale eddy in the Lofoten Basin of the Norwegian Sea during April 3–24, 2012. Initially, a vortex with a roughly circular shape undergoes deformation to the extent that its length becomes at least four times greater than its width. This signifies the transformation of the vortex into a filament. During this process, the kinetic energy decreases by a factor of three, the potential energy diminishes by an average of 1.7 times, and the overall energy of the vortex decreases by a factor of 2.3 [6].

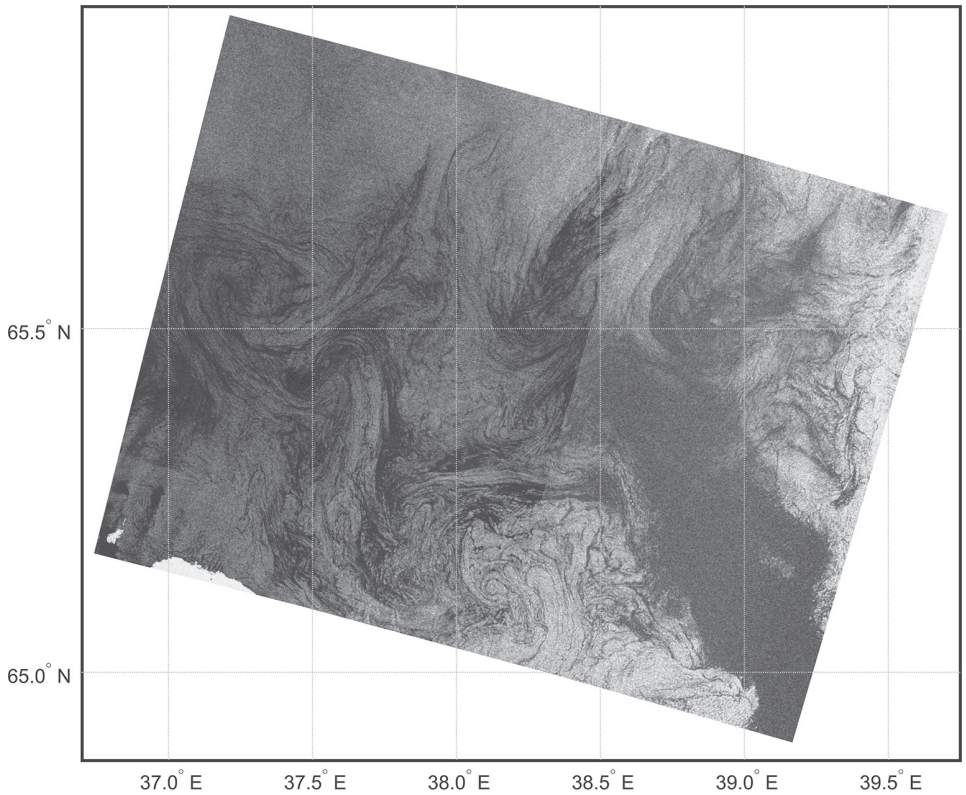

Fig. 1. Examples of filament occurrences in the White Sea, as observed in the Envisat ASAR radar image taken on June 24, 2010, at 08:11. UTC. © ESA

Another instance of such a transformation can be observed in [7] (for the animation, please refer to https://link.springer.com/article/10.1007/s00024-020-02647-1). The animation illustrates the process of filaments emerging from initially circular eddies that encircle the quasi-permanent anticyclonic Lofoten eddy in the Norwegian Sea.

Based on in-field observations and principles of fluid dynamics, an oceanic vortex consists of two main components: a central vortex core and a mass of seawater surrounding this core. The surrounding water also rotates in alignment with the core but at progressively slower speeds as it moves away from the core's outer edge. The orbital velocity in the core of the vortex increases as it moves away from the center of the core. It is maximal at the core boundary and decreases outside the core. Inside the eddy's core lies seawater that was trapped during the formation of the vortex, characterized by significantly higher vorticity compared to the surrounding background flow. An apt comparison for the core of a vortex is to imagine it as a "water-filled pocket." The core of the vortex moves harmoniously with the water in its immediate vicinity, which is why vortices have the capacity to transport water over considerable distances. The core's shape, usually delineated by its outer boundary, often experiences rotational changes, and the core itself can undergo deformation [8–12].

For ocean eddies with horizontal dimensions roughly equal to or larger than the inner Rossby deformation radius, the concept of potential vorticity conservation remains valid. Put simply, when these eddies travel, the individual particles inside them preserve their potential vorticity. This principle essentially reflects the conservation of angular momentum for fluid particles within a layered, rotating ocean environment.

1.1. Historical background

In 1899, the Russian scientist S.A. Chaplygin published a paper that investigated how a two-dimensional Kirchhoff vortex is deformed when subjected to a constant shear flow [13] (see also in [14]). Subsequently, these studies were further advanced in the field of planar hydrodynamics by Kida [15]. Later, generalizations of Kirchhoff's solution were proposed for a two-dimensional elliptical vortex with a piecewise-constant vorticity distribution [16]. Additionally, an approximate analytical solution was derived, accurate up to second order in a small Rossby number expansion, describing the shape of an arbitrarily oriented ellipsoid in an external flow with linear shear [17]. These works were extended to three-dimensional vortices by V.V. Zhmur [18] and also [19, 20]. These works delve into the dynamics of ellipsoidal vortices under various background conditions.

1.2. Ellipsoidal approximation of mesoscale vortices

In our study, we will approximate vortices with a co-rotating core in the form of an ellipsoid with two horizontal axes and one vertical axis. This is a more general form of vortex core than the traditional circular one. In the special case where the horizontal semi-axes of the ellipsoid coincide, our vortices become axisymmetric. The approach with ellipsoidal vortices allows us to investigate the deformation of vortices by external background flows. The problem of the behavior of ellipsoidal vortices in background barotropic flows was formulated and partially solved in the works [21, 22, 18], where it was shown that there are three regimes of behavior for such vortex cores. In two of these regimes, the vortex remains localized in the horizontal plane, undergoing periodic limited shape oscillations, specifically changes in the lengths of the horizontal semi-axes. In these regimes, the core shape rotates or oscillates around the vertical axis.

When a vortex undergoes deformation, its boundary can display three distinct behaviors: rotation, nutation oscillations, and unbounded elongation. In the first two scenarios, the eddy retains its localized structure. However, in the third case, one of its axes stretches infinitely while the other shrinks to zero. In the horizontal plane, such a vortex takes on the appearance of a vortex filament.

1.3. Stretching of a mesoscale vortex

We define the stretching of a mesoscale vortex as the process in which it elongates in a manner where its lengthwise dimension becomes greater than its width. The behavior of a vortex varies depending on whether it is within a barotropic background flow or a flow with vertical shear. In the presence of a background flow, and under specific conditions, a vortex can be stretched into a filament as it undergoes deformation. When a vortex experiences stretching in the horizontal plane, meaning its length becomes greater relative to its width, the fluid motion generated by the vortex weakens. From a physical standpoint, the scenario of unrestricted stretching signifies the vortex's disintegration due to the flow. Of particular interest is when the vortex, while interacting with the flow, deforms and stretches into a filament.

In these regimes, particle rotation within the core occurs either clockwise or counterclockwise, depending on whether we are considering cyclonic or anticyclonic vortex formation. The evolution of the core shape does not affect the direction of particle circulation within the core but does impact their magnitudes. The third, most interesting evolution regime for vortices in currents is the unbounded stretching of vortices in the horizontal plane by background flows. This behavior is accompanied by interesting hydrophysical phenomena, leading to the formation of long and thin vortex structures in the horizontal plane. As they stretch, these structures gradually lose their vortex properties: their circulation speeds decrease, both kinetic and potential energies diminish. According to theory [23], energy decreases both within the vortex cores and in the outer zone surrounding the core. Energy losses during vortex stretching have been confirmed by observational data [6, 24]. These energy losses are not related to friction. It is natural to expect that in geographical areas where vortices stretch, the energy lost by vortices is returned to the background flow.

A rigorous mathematical substantiation of the vortex stretching mode is meticulously detailed in the works [19, 20, 12, 24]. This justification builds upon the theory of mesoscale quasi-geostrophic eddies characterized by potential vorticity in the core, which takes the form of a deformable ellipsoid. Further advancements of these concepts can be found in articles authored by David Dritschel and his students (e. g., [25–28] and related references).

When mesoscale vortices are stretched within a deforming flow background, one can expect energy transfer from vortices to filaments, and subsequently, from mesoscale to submesoscale movements. This constitutes a direct energy cascade, closely associated with the unbounded stretching of vortices into filaments. Theoretical calculations suggest that significant elongation of the vortex core can lead to a reduction in vortex energy by 20–60 % [24]. Given that the physical system comprises solely vortices and a flow, it is reasonable to anticipate that the "lost" vortex energy will be redistributed back into the flow.

Returning to the concept of an ensemble of eddies as a manifestation of geophysical turbulence, where eddies originate from the flow and subsequently engage in energetic interactions with it, this phenomenon of energy recovery from turbulence within the flow is referred to as the reverse energy cascade, or alternatively known as the "negative viscosity phenomenon" [29].

2. Research Objectives

The primary objective of this study is to elucidate the physical conditions that lead to the transformation of eddies into elongated filaments within the World Ocean. This transformation is driven by the influence of uniformly vortical

background flows, which exhibit linearity in horizontal coordinates. Additionally, we aim to quantify the proportion of mesoscale eddies undergoing this elongation process, ultimately facilitating the redistribution of energy from the mesoscale to the submesoscale.

3. Basics of the theory

The foundational principles of ellipsoidal vortex theory are comprehensively outlined in various works (see the reference list in [18]). In this approach, the change in the shape of vortex cores is associated with the deforming properties of large-scale currents, namely, the presence of a nonzero deformation coefficient in the currents. The alteration of the vortex core shapes in response to the deforming properties of the currents is a key aspect in understanding vortex evolution in hydrodynamic flows. Let's delve into this thesis in more detail.

If the characteristic horizontal size of background barotropic flows noticeably exceeds the horizontal size of vortex nuclei, then it is permissible to decompose the background flow field $\vec{u}_b(x,y) = \left(u_b(x,y), v_b(x,y)\right)$ in Taylor's row in the vicinity of the vortex center $(x_0(t), y_0(t))$, where $u_b(x, y)$ and $v_b(x, y)$ are the background components of the velocity field. In this case, we can limit to linear terms in horizontal coordinates:

$$\begin{aligned} u_b(x,y) &= u_b(x_0,y_0) + e_1(x-x_0) - \gamma_1(y-y_0), \\ v_b(x,y) &= v_b(x_0,y_0) + \gamma_2(x-x_0) - e_1(y-y_0). \end{aligned} \tag{1}$$

Here x and y are horizontal coordinates. The signs of the set of the coefficients $\begin{pmatrix} e_1 & -\gamma_1 \\ \gamma_2 & -e_1 \end{pmatrix}$ in (1) are chosen for convenience reasons for further use. In this case, the incompressibility condition $\frac{\partial u_b}{\partial x} + \frac{\partial v_b}{\partial y} = 0$ is done automatically by default, and $(\gamma_1 + \gamma_2) = rot_z \vec{u}_b(x,y)$. The coefficients e_1, γ_1, γ_2 will change when rotating the coordinate system (x, y). However, there is always a coordinate system in which the coefficients γ_1 and γ_2 are equal, i. e. $\gamma_1 = \gamma_2 = \gamma$. The coefficient e_1 in the same coordinate system will take some value e. As a result, the matrix $\begin{pmatrix} e_1 & -\gamma_1 \\ \gamma_2 & -e_1 \end{pmatrix}$ will take a simpler form $\begin{pmatrix} e & -\gamma \\ \gamma & -e \end{pmatrix}$. The coefficient $\gamma = \frac{1}{2} rot_z \vec{u}_b(x,y)$ is the angular velocity of rotation of the fluid particles of the background flow, and the coefficient e, called the deformation coefficient, is responsible for the deformation properties of the background flow. Such flows are called flows with equal vorticity, in which the behavior of ellipsoidal vortices was studied [21, 22, 18]. The properties of ellipsoidality and equal vorticity of background flows make it possible to write out the main physical characteristics of vortices in the form of algebraic relations, which significantly simplifies the study. In the absence of background flow, the vortex does not deform, and its shape (ellipsoid) rotates around a vertical axis with a constant angular velocity. The particles in the core overtake the rotation of the shape. The presence of a non-zero deformation coefficient e leads to a change in the shape of the core. At the same time, the vortex itself moves as a whole with the speed of an undisturbed background flow. The presence of movement as a whole has nothing to do with vortex deformation.

Then, we consider the barotropic flow $\vec{u} = (u, v, 0)$ with the linear dependence of the flow velocity on the horizontal coordinates:

$$\vec{u} = (u,v,0) = \begin{cases} u = u_0 + ex - \gamma y \\ v = v_0 + \gamma x - ey \end{cases}. \tag{2}$$

Here u_0 and v_0 are the flow velocity components in the vortex center $x = 0$, $y = 0$. In such a flow, the center of the vortex moves, as a whole, with the speed of the external flow (u_0, v_0) and simultaneously rotates and deforms. We are only interested in the deformation component of the vortex evolution. The relations (2) include two flow parameters, i. e. e and γ. Both of them describe the inhomogeneity of the flow, i. e. the dependence of the flow on the coordinates. The coordinate system for equations (2) is chosen in such a way that the coefficients for the y-component of velocity (i. e. — γ) and for the x-component of velocity (i. e. γ) are the same in modulus, but opposite in sign, so $e = \frac{\partial u}{\partial x} = -\frac{\partial v}{\partial y}$ follows from the divergence-free flow (2). This type of coordinate system can always be derived from any other coordinate system with a vertical axis z, where the velocity vector has an arbitrary linear relationship with the horizontal coordinates of the barotropic flow. This is achieved by rotating the coordinate system around the ver-

tical axis *z*. Kida [15] employed what is commonly known as the "convenient" coordinate system when investigating the evolution of the Kirchhoff vortex within the flow. The relevance of the chosen coordinate system to the general case of an arbitrary coordinate system or the traditional coordinate system used in oceanography, where the *x*-axis points East, the *y*-axis points North, and the *z*-axis is vertical, is clarified in Appendix III. In the case of barotropic flow, the center of the vortex moves with the velocity of the external flow, converging at the center of the ellipsoid. The vertical semi-axis (c) remains constant, while the horizontal axes undergo changes so that the product $a(t) \times b(t)$ is preserved where *a* is the large semi-axis, *b* is the small semi-axis, and *c* is the vertical semi-axis of the ellipsoid.

The potential vorticity of the background flow in terms of flow parameters is 2γ. The potential vorticity describes different types of flows at different ratios of *e* and γ. When $|\gamma| > |e|$, the background flow is a movement along closed current lines in the form of ellipses. When $|\gamma| = |e|$, the background flow is a rectilinear flow with a shift. When $|\gamma| < |e|$, the current lines of the background flow are a set of hyperbolas.

The problem is reduced to the evolution in time of two horizontal semi-axes of the ellipsoid $a(t)$ and $b(t)$, i. e. to a system of two differential equations for the ratio of the semi-axes $\varepsilon = \frac{a}{b}$ and orientation angle θ of the larger horizontal semi-axis of the ellipsoid *a* to the coordinate axis *x* (see please proof in [18]). In the general case, the variable intrinsic angular velocity of rotation of the shape of the vortex core $\Omega(\varepsilon, K)$ depends on the horizontal elongation of the vortex core $\varepsilon = \frac{a}{b}$ and the parameter of the vertical oblateness of the vortex core $K = \frac{N}{f}\frac{c}{\sqrt{ab}}$, where *N* is the Väisälä-Brunt frequency, *f* is the Coriolis parameter, and *c* is the vertical semi-axis. The change in the core shape is a result of the deformation coefficient *e* in the background flow (1). Physically, the deformation of the core shape is attributed to the spatial non-uniformity or variability in the background flow, and σ is the excess potential vorticity of the vortex core over the potential vorticity 2γ background flow (1). A discussion about potential vorticity is given in Appendix I.

When transitioning to dimensionless variables, it becomes evident that on the phase plane (ε, sin2θ). The trajectory of the integral curve, which describes the evolution of a vortex, is contingent on three dimensionless parameters: γ/e, σ/e and *K*. The advantage of utilizing a dimensionless set of variables γ/e, σ/e, and *K* is as follows: γ/e pertains solely to the description or characterization of the background flow, σ/e shows the relative intensity of the vortex, and *K* Is the geometric factor that describes the vertical flatness of the vortex core. Small values $K < 1$ correspond to thin vortices, and large values $K > 1$ correspond to thick ones. When subjected to barotropic flow (1), the parameter K remains constant, even as the vortex core undergoes deformation. The deformation of the core shape is a result of the deformation coefficient "e" in the background flow (1), and it is also influenced physically by the spatial non-uniformity of the background flow. When calculating the parameter $\left|\frac{\gamma}{e}\right|$, only the effect of the background flow (and the exclusion of vortex dynamics) is considered. We used the smoothing of geostrophic velocity fields by the moving average method with a window of a width of 1° × 1°. A moving average smoothes the data by consolidating the spatial data points into longer units of space (see please [30]).

For constant coefficients "e" and "γ," the system of differential equations is solved using quadrature methods [18]. As a result of this solution, it is derived that any integral curve in the parameter plane (e; sin2q) describes the evolution of a specific vortex, contingent upon the background flow parameters "e" and "γ," the vertical oblateness parameter of the vortex core "K," and the integration constant "C," subject to a physical constraint: $|\sin 2\theta| \le 1$. A rigorous mathematical derivation of the relevant formulas can be found in [18, 5, 31, 32]. It's worth highlighting that in this context, the plane (ε; sin2θ) is the phase plane. In the context of the flow described by formula (1), there are three possible behaviors for the shape of ellipsoidal vortices:

(1) Two periodic modes: These include the rotation mode and the mode where the core shape oscillates periodically.

(2) The mode of unlimited elongation of the core in the horizontal direction: This occurs under the influence of uniformly vortexed linear flows in coordinates.

These behaviors are observed within the plane of study.

In the realm of ellipsoidal vortex theory, we utilize a previously established map depicting the theoretical behavior of vortices in barotropic flows, employing dimensionless coordinates for convenience. A key finding from this map is the existence of a region denoting imminent vortex stretching, represented by the color purple. Rather than delving into the theory itself, we rely on it, drawing upon [5, 31, 32]. The constancy of the parameter *K* for each vortex enables us to investigate the presence of each of the three modes (rotation, nutation oscillations, and unlimited extension) characterizing vortex behavior within the parameter plane. (γ/e, σ/e). Figure 2 shows for the selected value $K = 0.2$ the structure of zones with different behavior of phase trajectories on the parameter plane (γ/e, σ/e). According to the theory, the parameter *K* remains constant during the evolution of vortices in barotropic flows.

However, it can vary from one vortex to another, and it may also change over time in response to fluctuations in the Väisälä-Brunt frequency. We have chosen a characteristic value of K as 0.2, which represents a typical value for the majority of mesoscale vortices.

In the ocean, the characteristic value of the ratio N/f is approximately 20. The ratio of the vertical scale to the horizontal scale for vortices is relatively small, typically around 0.01, which means that the product of 20 × 0.01 equals 0.2. If the horizontal dimensions of the vortices increase, the value of K becomes even smaller. Conversely, decreasing the horizontal dimensions is associated with a reduction in vertical dimensions, but the overall value of K remains in the order of 0.2.

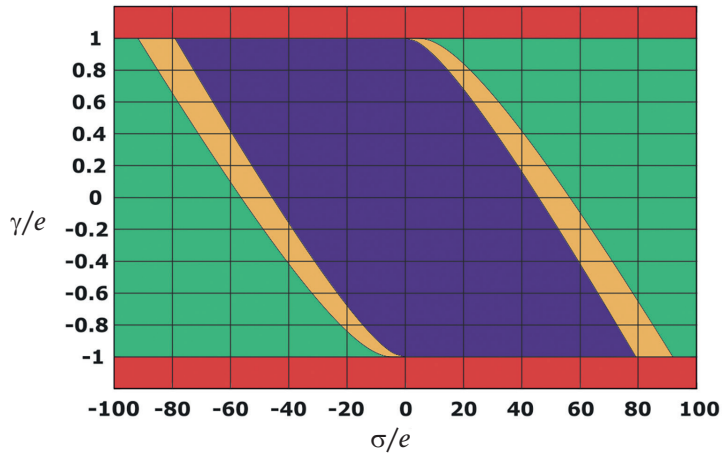

Fig. 2. In the parameter plane (σ/e, γ/e), there are three distinct modes of behavior for vortices, and they are separated by four curves that originate in pairs from specific points with $K = 0.2$ [5]

These modes are as follows:

Rotation Mode: Vortices primarily exhibit rotation behavior. This mode is represented by one of the three distinct areas in the parameter plane.

Nutation Oscillation Mode: Vortices display nutation or oscillatory behavior. This mode is represented by another distinct area in the parameter plane.

Unlimited Extension (Horizontal) Mode: Vortices elongate significantly in the horizontal direction. This mode is the third distinct area in the parameter plane.

The four curves, which emerge in pairs from specific points, serve as boundaries or transitions between these three modes. These curves define the regions where one mode transitions into another. The specific coordinates and equations for these curves would be determined by the characteristics of the study and the equations governing vortex behavior.

Three distinct areas are identified along the ordinate (vertical) axis, with each area having specific characteristics or behaviors $|\gamma / e| > 1$, there are only oscillatory and rotational modes (red color, the area extends to infinity); in the area of $|\gamma / e| \le 1$, all three modes are allowed, which are separated from each other by four curves emerging in pairs from points $(0; \pm 1)$ and $\left(\pm \left(\frac{\sigma}{e} \right)_0, \pm 1 \right)$.

As a result, the strip $|\gamma / e| \le 1$ is divided into three zones symmetrical concerning the origin:

• In the parameter plane, there is an external (green) region where all three modes of vortex behavior are allowed: rotational, oscillatory, and elongating. This external green region encompasses the entire parameter space, indicating that vortices within this area can exhibit any of the three modes of behavior without any specific restrictions.

• In the parameter plane, there is an intermediate (yellow) region where only two modes of vortex behavior are allowed: oscillatory and unlimited stretching. Vortices within this yellow region can exhibit either oscillatory behavior or unlimited stretching behavior, but rotational behavior is not observed in this zone.

• In the parameter plane, there is an internal (purple) region where only one mode of vortex behavior is allowed: unlimited vortex core stretching. Vortices within this purple region predominantly exhibit the behavior of elongating their core in an unlimited manner. Rotational and oscillatory behaviors are not observed within this zone.

Qualitatively, this behavior can be explained as follows:

According to the equations describing the evolution of vortices in a flow (as presented in [18]), two key factors influence the vortex shape:

(1) Intrinsic Rotation: The vortex shape inherently rotates on its own.

(2) External Flow Interaction: Additionally, the vortex shape is further twisted by the rotational component of the external flow.

The elongation of the vortex is closely related to its rotation. For the vortex to elongate continuously, it requires a significant reduction in the rotation of its shape. This reduction in rotation occurs when the signs of the potential vorticity parameter (σ) and the parameter (γ) representing the external flow's rotational component are different.

In other words, when σ and γ have opposite signs, they tend to counteract each other's rotational effects, leading to the elongation of the vortex core. This explains why the internal (purple) region in the parameter plane is associated with unlimited vortex core stretching since in this region, the signs of σ and γ are such that they minimize the rotation of the vortex's shape, allowing for its elongation.

Indeed, when the signs of the potential vorticity parameter (σ) and the parameter (γ) representing the external flow's rotational component are the same, several key behaviors result:

(1) Independent Rotation: The vortex rotates independently, maintaining its intrinsic rotational characteristics.

(2) Additional Twisting by Flow: The vortex shape is additionally twisted by the external flow in the same direction, amplifying its rotation.

As a consequence of this behavior, vortices with the same signs of σ and γ tend to reinforce their rotational tendencies, making it challenging for them to elongate indefinitely. This is why, in the parameter plane, points corresponding to vortices with the same sign of vorticity are situated in the rotation zone. This zone signifies that these vortices maintain their rotation rather than elongate significantly.

Conversely, weaker vortices with different signs of σ and γ experience a different outcome. These vortices are primarily stretched by the flow, leading to the formation of vortex filaments. Conversely, vortices with the same signs of σ and γ are not stretched significantly by deformation flows.

This phenomenon explains the presence of weaker, smaller vortices with opposite signs of vorticity in the vicinity of larger, more intense eddies. The weaker vortices, when close to the intense vortex of the same sign, tend to be drawn out into filaments due to their susceptibility to stretching by the flow. This behavior aligns with the observations and findings discussed in [7, 33–35].

Thus, when $|\gamma / e| \le 1$, a stretching mode is allowed, but only a stretching mode exists in the zone colored in purple in Fig. 2. Indeed, when the conditions align such that σ and γ have certain relationships, primarily when they differ in sign, a stretching mode becomes allowed. In the purple-shaded zone on Fig. 2, only this stretching mode is observed, indicating that vortices in this region predominantly exhibit the behavior of stretching their cores.

The availability of real-world information about the current field in various regions of the World Ocean allows for the empirical determination of which regime (rotation, oscillation, stretching, or a combination thereof) is realized in specific areas. These empirical findings can provide valuable insights into the behavior of vortices in different oceanic regions. Despite the fact that the presented theory relates to the parameter $K = 0.2$, these results can be extended to other parameters of the vertical flatness of the vortex if the dimension theory is applied. More details are provided in the Appendix II.

The results of this empirical analysis, which identify the dominant vortex behavior in various parts of the World Ocean, are expected to be presented in one of the upcoming sections. These findings will contribute to a better understanding of mesoscale oceanic phenomena and their impact on ocean circulation and dynamics.

4. Data and Methods

To achieve the objectives of the study, we rely on satellite altimetry data, which are compiled by merging measurements from various altimetry missions, including Jason-3, Sentinel-3A, HY-2A, Saral/AltiKa, Cryosat-2, Jason-2, Jason-1, TOPEX/Poseidon, Envisat, GFO, ERS1/2. We utilized Sea Level Anomalies (SLA) and geostrophic velocity components derived from dynamic topography data (ADT). These datasets were obtained from the Copernicus Marine Environment Monitoring Service (CMEMS) portal (http://marine.copernicus.eu/). The data is a comprehensive compilation of measurements from various altimetry missions, including missions such as Jason-3, Sentinel-3A, HY-2A, Saral/AltiKa, Cryosat-2, Jason-2, Jason-1, TOPEX/Poseidon, Envisat, GFO, and ERS1/2, spanning from 1993 to the present.

This SLA data is a result of an interpolated dataset CMEMS with a spatial resolution of 0.25 degrees for both latitude and longitude. The data is provided at a temporal interval of 1 day, as outlined in [36]. The most recent update

of the dataset incorporates several improvements. These include the addition of a new sensor and atmospheric corrections, recalibration of various altimeters, the integration of a new tide model, and an extension of the base period for estimating mean sea level to 20 years, as documented in [37].

For this dataset, Sea Level Anomalies (SLAs) were computed relative to the Mean Sea Surface (MSS) data, which is accessible through the Aviso+ portal (Archiving, Validation, and Interpretation of Satellite Oceanographic Data, http://www.aviso.altimetry.fr/en/data/products/auxiliary-products/mss.html). The altimetry data covers the period from 1993 to 2021. These enhancements and the utilization of the updated MSS data contribute to the accuracy and comprehensiveness of the dataset, making it valuable for various applications related to oceanography and sea level analysis over this 28-year period.

In this work, we also use the data of the regional hydrodynamic model of the MITgcm (Massachusetts Institute of Technology General Circulation Model) with a horizontal spatial resolution of about 4 km and 50 layers from 10 m in thickness near the surface to 456 m near the bottom. A description of the model can be found in [38]. Oceanic boundary conditions were taken from the optimal implementation of the global ECCO2 model, and the initial conditions were taken from the World Ocean Atlas 2009 database. As forcing, the model uses atmospheric reanalysis data JRA55 (Japanese 55-year Re-analysis).

In the context of studying the impact of background flow on vortices, an essential parameter is the dimensionless number $|\gamma/e|$, which characterizes the properties of background flow inhomogeneities. However, when attempting to calculate $|\gamma/e|$ using altimetry data, where currents and vortices are intertwined, it becomes necessary to distinguish between the properties of currents and vortices. In this research paper, we employ a relatively straightforward approach to address this issue. In the first step, we extract the values of the desired characteristics from the 0.25° altimetric data grid and place them onto a coarser 1° grid. This process results in the majority of vortices being filtered out, as they fall into the coarser subgrid area. Nonetheless, some vortices still intersect with the nodes of the 1° grid, introducing a degree of error into the analyzed flow. However, the averaging process smooths out the spatial inhomogeneities in the flow itself, making the real properties of the flows align more closely with the theoretical requirements of large-scale flows. While it's important to acknowledge that complete separation of flow fields from vortex fields is not achievable through this method, it does significantly reduce the influence of vortices on the parameters γ and e. Consequently, it also diminishes the significance of vortex effects on the final parameter $|\gamma/e|$ characterizing the background flow.

5. Results

Mesoscale vortices are one of the most common dynamic structures of the World Ocean, covering about 1/3 of its area [1, 39]. In this section, we do not analyze the features of vortex formation in a particular region of the World Ocean and its regional specifics considering various regions just as examples. We also do not analyze the spatial and temporal variability caused by mesoscale vortices. We are interested in a property of vortices in the ocean that has not been studied before, namely, the ability of vortices to stretch into filaments. We demonstrate this property for one randomly selected date July 1, 2022. We believe that choosing a different date will not significantly change the estimates obtained. We consider the property of vortices to elongation for the World Ocean and for individual regions, the choice of which in this study also does not matter significantly.

We proceed to calculate the proportion of mesoscale eddies that undergo unlimited elongation into submesoscale filaments under the influence of a barotropic current in different regions of the World Ocean. For this analysis, we shift to a geographical coordinate system where the x-axis is oriented to the east, and the y-axis is oriented to the north. In Figure 3, we observe a patchy distribution across the World Ocean, with regions exhibiting properties $|\gamma/e| > 1$ (indicating that vortex stretching into filaments is not allowed) and properties $|\gamma/e| < 1$ (representing the regime of unrestricted vortex stretching).

This analysis seeks to quantify the prevalence of mesoscale eddies transitioning into submesoscale filaments in various oceanic areas, shedding light on the geographical distribution of this phenomenon and its implications for ocean dynamics.

Estimates of domain scales at latitudes around 30° North and South indicate that the characteristic size of the "spots" is approximately 200 kilometers. Meanwhile, the size of the larger "spots" with a brown color $\left(\left|\frac{\gamma}{e}\right| > 1\right)$ is less than the size of large "spots" of blue $\left(\left|\frac{\gamma}{e}\right| < 1\right)$. It means that $S_{\leq 1}$ — the integral areas of the regions corresponding to the regime of unrestricted elongation of mesoscale vortices into filaments are greater than the areas of regions where

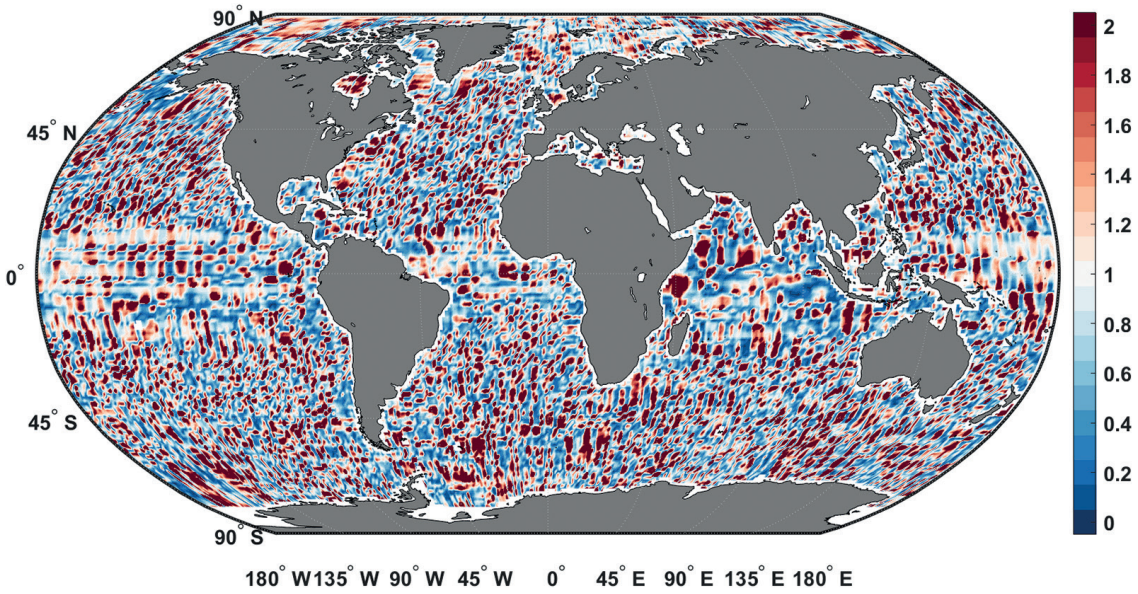

Fig. 3. The geographical distribution of the parameter $\left|\frac{\gamma}{e}\right|$ in the World Ocean was obtained from altimetry data using spatial averaging via the moving average method with a window width of 1°. This data is dated July 1, 2022, and it provides insights into how this parameter varies across different oceanic regions. In this representation, a brown color is used to denote spots with a certain characteristic $|\gamma/e| > 1$, indicating that vortex stretching into filaments is prohibited. On the other hand, a blue color is employed for spots with a different characteristic $|\gamma/e| < 1$, signifying that the regime of unlimited vortex stretching is taking place in those regions. These color distinctions help visualize the distribution of vortex behavior in the World Ocean based on the specified criteria

elongation is prohibited. Indeed, our estimates demonstrate a specific ratio $S_{\leq 1}$ to the total surface area S of the World Ocean $\frac{S_{\leq 1}}{S} = 0.60$. When we calculate the same ratio using altimeter data with a spatial resolution of 0.25 degrees, we obtain $\frac{S_{\leq 1}}{S} = 0.66$. The ratio of the integral areas represented by the blue color $S_{\leq 1}$ and the areas of brown color $S_{>1}$ on a one-degree grid without averaging is $\frac{S_{\leq 1}}{S_{>1}} \approx 1.9$, and it is $\frac{S_{\leq 1}}{S_{>1}} \approx 1.5$ with spatial averaging. From the analysis, it can be deduced that the integral area of the World Ocean domains where eddies can elongate is larger than the integral area of domains where elongation is prohibited. The estimated ratio of areas, both with and without field averaging, is expressed as follows:

$$1.5 < \frac{S_{\leq 1}}{S_{>1}} < 1.9, \tag{3}$$

$$0.60 < \frac{S_{\leq 1}}{S} < 0.66. \tag{4}$$

It's important to note that the maps (Fig. 3–5) are considered for a single date each and that the spatial smoothing is applied individually for each date. To assess the seasonal variations and interannual variability in the spatial distribution of the parameter $\left|\frac{\gamma}{e}\right|$, we conducted analyses using appropriate time-averaging techniques for the period spanning from 1993 to 2021. The results of these averaged calculations are presented in Tables 1 and 2, allowing us to gain insights into the parameter's behavior over this extended time frame.

Hence, the ratio of integral areas across various types of domains displays minimal variation from one season to another. This consistency is maintained even during interannual fluctuations, as evidenced by the data presented in Table 2.

Table 1

The seasonal variations in the ratios of integral areas corresponding to different types of domains

	World Ocean		Northwest Pacific		Arabian Sea and the Bay of Bengal	
Season	$S_{\le 1}/S_{>1}$	$S_{\le 1}/S$	$S_{\le 1}/S_{>1}$	$S_{\le 1}/S$	$S_{\le 1}/S_{>1}$	$S_{\le 1}/S$
Winter	1.49	0.60	1.73	0.63	1.18	0.54
Spring	1.49	0.60	1.68	0.63	1.43	0.59
Summer	1.48	0.60	1.65	0.62	1.77	0.64
Autumn	1.44	0.59	1.64	0.62	1.52	0.60

Table 2

The interannual variability in the ratios of integral areas corresponding to different types of domains

	World Ocean		Northwest Pacific Ocean		Arabian Sea and the Bay of Bengal	
Year	$S_{\le 1}/S_{>1}$	$S_{\le 1}/S$	$S_{\le 1}/S_{>1}$	$S_{\le 1}/S$	$S_{\le 1}/S_{>1}$	$S_{\le 1}/S$
1993	1.51	0.60	1.91	0.66	1.49	0.60
1994	1.49	0.60	1.92	0.66	1.52	0.60
1995	1.52	0.60	1.83	0.65	1.43	0.59
1996	1.48	0.60	1.75	0.64	1.43	0.59
1997	1.50	0.60	1.86	0.65	1.35	0.58
1998	1.54	0.61	1.97	0.66	1.39	0.58
1999	1.47	0.60	1.86	0.65	1.30	0.57
2000	1.48	0.60	1.99	0.67	1.47	0.60
2001	1.48	0.60	2.09	0.68	1.58	0.61
2002	1.49	0.60	1.83	0.65	1.45	0.59
2003	1.49	0.60	1.99	0.67	1.48	0.60
2004	1.49	0.60	1.85	0.65	1.34	0.57
2005	1.51	0.60	2.11	0.68	1.44	0.59
2006	1.49	0.60	1.96	0.66	1.31	0.57
2007	1.51	0.60	1.78	0.64	1.74	0.64
2008	1.50	0.60	1.73	0.63	1.27	0.56
2009	1.49	0.60	1.69	0.63	1.36	0.58
2010	1.48	0.60	1.62	0.62	1.63	0.62
2011	1.51	0.60	1.69	0.63	1.66	0.62
2012	1.50	0.60	1.71	0.63	1.57	0.61
2013	1.51	0.60	1.95	0.66	1.42	0.59
2014	1.48	0.60	2.08	0.68	1.49	0.60
2015	1.49	0.60	2.08	0.68	1.30	0.56
2016	1.50	0.60	1.65	0.62	1.46	0.59
2017	1.56	0.61	1.98	0.66	1.60	0.62
2018	1.50	0.60	1.66	0.62	1.40	0.58
2019	1.50	0.60	1.93	0.66	1.39	0.58
2020	1.49	0.60	1.90	0.65	1.43	0.59
2021	1.50	0.60	1.99	0.67	1.50	0.60
The averages calculated for the period spanning from 1993 to 2021.	1.50	0.60	1.69	0.63	1.40	0.58

Figures 4–6 depict the spatial distributions of domains with distinct characteristics within specific regions of the World Ocean. These figures provide visual insights into how these properties vary across various oceanic areas. Table 1 depicts the seasonal variability of $S_{\le 1}/S_{>1}$ and $S_{\le 1}/S$ distributions for the World Ocean, Northwest Pacific, Arabian Sea, and the Bay of Bengal individually. Table 2 demonstrates the interannual variability of $S_{\le 1}/S_{>1}$ and $S_{\le 1}/S$

distributions for these basins. They reveal the insignificant seasonal and interannual variability inside every basin because there are small differences in values of these characteristics. However, there are differences for the various areas which is understandable since the intensity of the vortex dynamics varies for different areas. Figures 4 and 5 demonstrate these distributions for the chosen date (July 1, 2022) as well as for the different seasons which correspond to the values in Table 1.

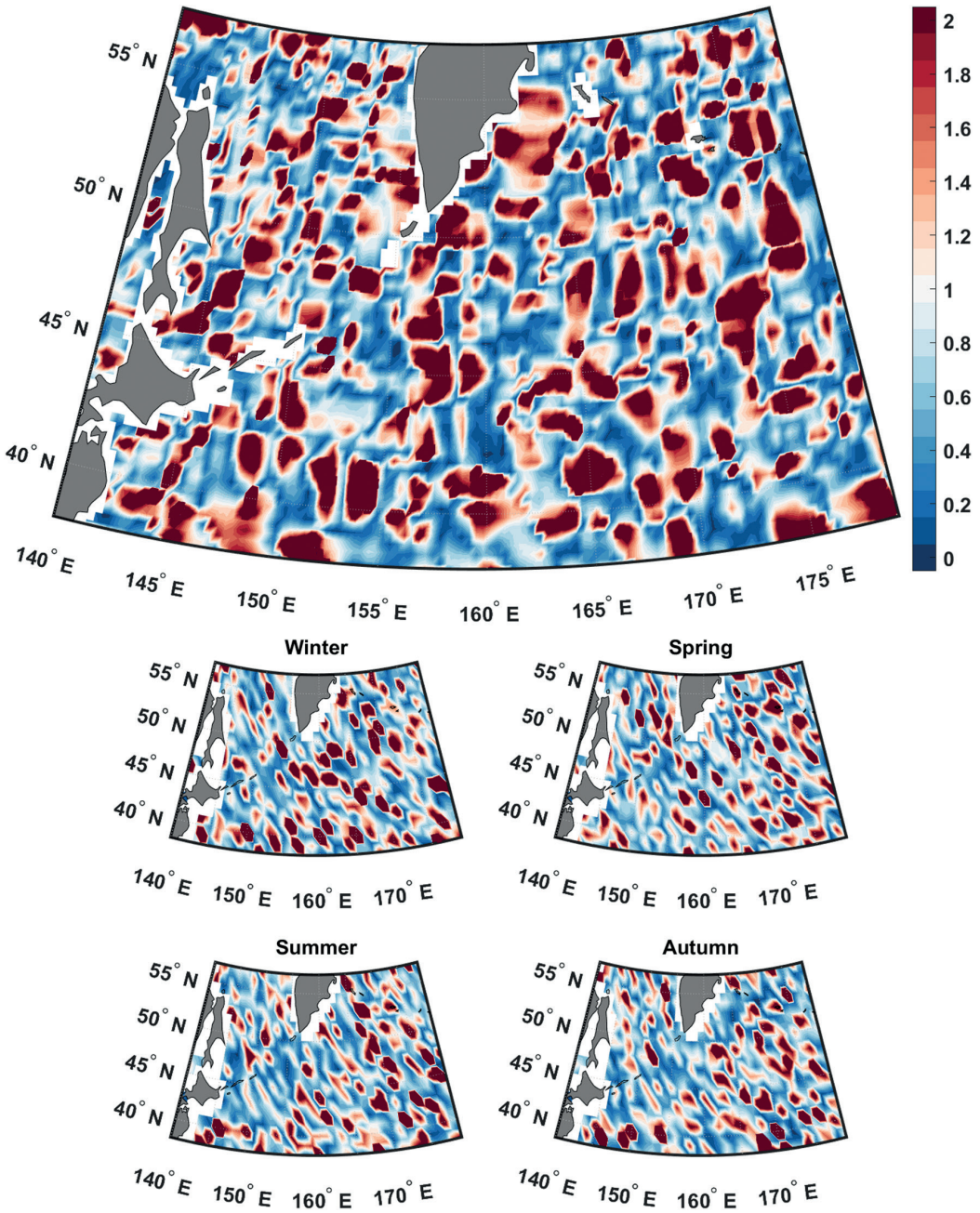

Fig. 4. The geographical distribution of the parameter $\left|\frac{\gamma}{e}\right|$ for the Northwest Pacific was derived from altimetry data using spatial averaging via the moving average method with a window width of 1°. The top figure presents the distribution for July 1, 2022, and the lower figures demonstrate the seasonal variability for 1993–2021. A brown color is indicative of spots with a specific characteristic $|\gamma/e| > 1$, denoting that vortex stretching into filaments is prohibited. Conversely, the blue color is used to designate spots with a different characteristic $|\gamma/e| < 1$, signifying that the regime of unlimited vortex stretching is occurring in those regions. These color distinctions help visualize the distribution of vortex behavior within the Northwest Pacific Ocean based on the specified criteria

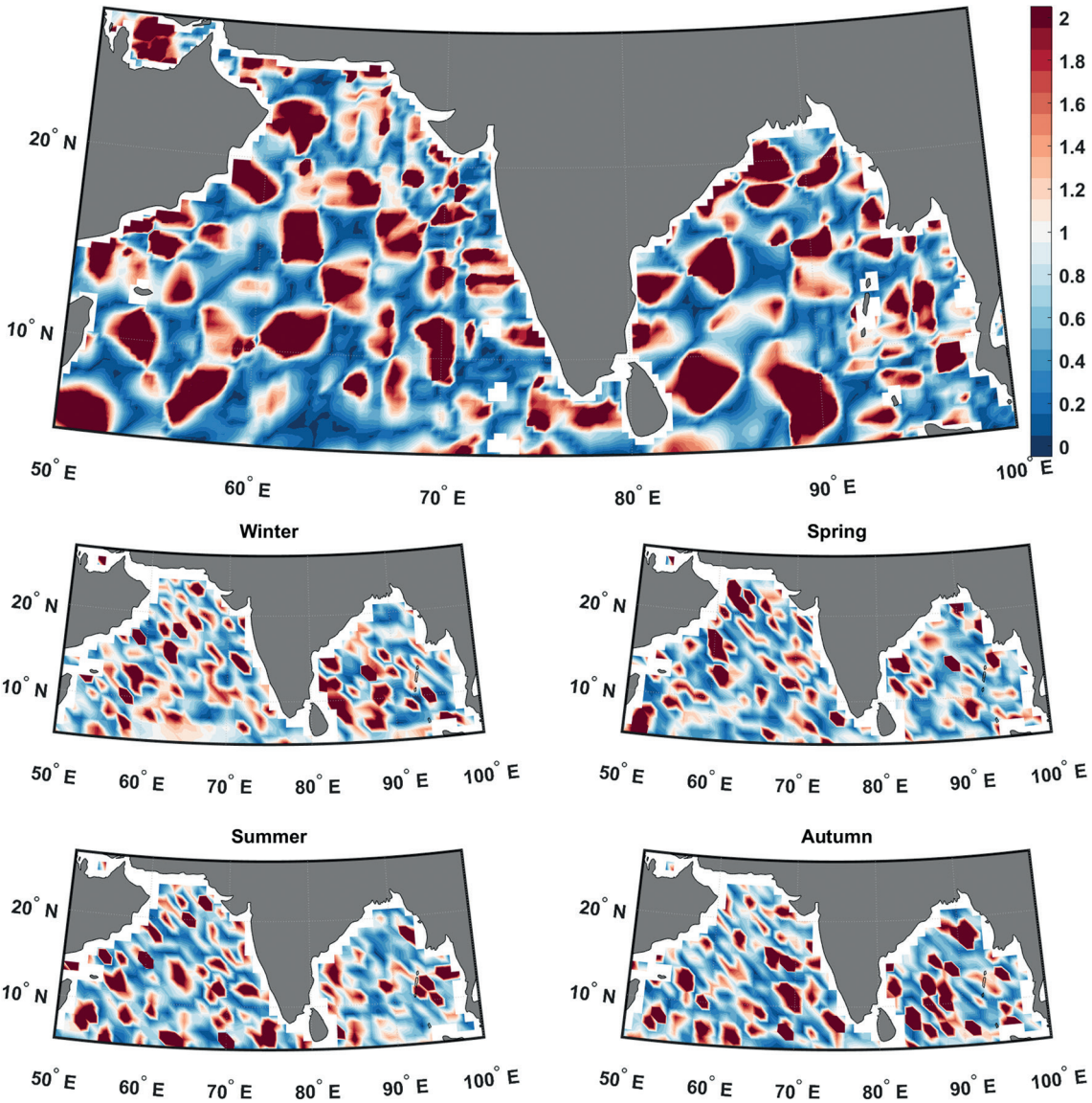

Fig. 5. The geographical distribution of the parameter $\left|\frac{\gamma}{e}\right|$ for the Arabian Sea and the Bay of Bengal of the Indian Ocean was derived from altimetry data using spatial averaging via the moving average method with a window width of 1°. The top figure presents the distribution for July 1, 2022, and the lower figures demonstrate the seasonal variability for 1993–2021. A brown color is indicative of spots with a specific characteristic $|\gamma/e| > 1$, denoting that vortex stretching into filaments is prohibited. Conversely, the blue color is used to designate spots with a different characteristic $|\gamma/e| < 1$, signifying that the regime of unlimited vortex stretching is occurring in those regions

It's noteworthy that the ratio of integral domain areas $S_{\leq 1}$ (representing vortex stretching and other properties) to the total area of the ocean (S) has exhibited remarkable stability, consistently remaining at 60 %. This finding implies that mesoscale eddies in the ocean have the capacity to stretch, but the overall integral areas where this property is observed remain relatively constant.

Therefore, we observe another conservation principle at play, which we refer to as the "law of conservation of the integral area of the World Ocean," where the ratio of integral domain areas to the total ocean area remains approximately constant at 60 %. This signifies that regions in the World Ocean where mesoscale eddies can elongate into vortex filaments maintain their overall integral area over time. Similarly, the integral area of regions where stretching is prohibited remains conserved. Typically, these regions correspond to areas where quasi-stationary eddies are located, such as the Lofoten Basin eddy (as discussed in [30, 40], or in areas where large rings are formed, such as the Agulhas Current region (as observed in [41, 42]). This conservation phenomenon suggests that these regions with specific eddy characteristics maintain their integral areas consistently over time.

6. Discussion and Conclusion

Within mesoscale vortices, the field of relative vorticity tends to remain relatively uniform because the development of filaments within the cores of these vortices is limited. While filaments can form outside the vortices, they tend to dissipate quickly due to diffusion. As a result, dynamically active regions like the Agulhas, Gulf Stream, and Kuroshio may contain areas with both filamentary structures and smoother features.

The question arises: do the regions $|\gamma/e| > 1$ really identify the property of ocean dynamics, where there is a prohibition of vortices to elongation? For this purpose, we compare the various characteristics characterizing the presence of a vortex in a given area with standard parameters that are commonly used in vortex analysis. We are talking about relative vorticity and the Okubo-Weiss parameter. The object of comparison is a quasi-permanent anticyclonic Lofoten vortex. A notable feature of the Lofoten anticyclone is that it has a topographic nature and is quasi-permanent. This means that the vortex is constantly in approximately the same place.

The Lofoten Vortex is of great interest to researchers, being a unique natural laboratory for studying vortices in nature. It is represented by a lens of warm salt water at a depth interval of 300–1000 m with a horizontal scale of about 60–80 km. According to glider data, the radius of the vortex core is 18 ± 4 km [43]. The existence of a quasi-constant anticyclonic Lofoten Vortex in the basin is confirmed by in situ measurements [11, 43–49], satellite data [30, 33, 50–52], and hydrodynamic modeling data [33, 38, 48, 53–58]. Its most probable location in the Lofoten Basin is limited to 69°–70° N and 2°–5° E. The Lofoten Vortex is in continuous motion mainly along isobaths in a cyclonic direction at a speed of 3–4 cm/s relative to the center of the basin. The maximum orbital velocities in the vortex are 50–70 cm/s.

Let's focus on the stretching impact of the flow near the Lofoten anticyclone. In this context, "flow" encompasses the combined influence of the background flow and the flow generated by the Lofoten vortex itself. This combination of flows leads to the creation of elongated vortices in the vicinity of the Lofoten anticyclone. Figure 6a displays the relative vorticity field in the mid-flow. In the depicted figure, the vortex core is characterized by a negative vorticity on the order of -3×10^{-5} s^{-1}, represented by the blue color. In the vicinity of the vortex, there are regions with positive vorticity of a similar order, indicated by the brown color. The Rossby number in this area does not exceed 0.25 (with the Coriolis parameter $f = 1.371\times10^{-4}$ s^{-1} at 70° N). Furthermore, the analysis includes the calculation of the strain rate or deformed flow field, following the Okubo-Weiss formulation (as described in [59, 60]). This additional analysis provides insights into the deformation characteristics of the flow field within this region (Fig. 6b): $W = s_n^2 + s_s^2 - \zeta^2$, where $\zeta = \frac{\partial v}{\partial x} - \frac{\partial u}{\partial y} = \frac{g}{f}\left(\frac{\partial^2 h}{\partial x^2} + \frac{\partial^2 h}{\partial y^2}\right)$ is the relative vorticity, $s_n = \frac{\partial u}{\partial x} - \frac{\partial v}{\partial y} = -\frac{2g}{f}\frac{\partial^2 h}{\partial x \partial y}$ and $s_s = \frac{\partial v}{\partial x} + \frac{\partial u}{\partial y} = \frac{g}{f}\left(\frac{\partial^2 h}{\partial x^2} - \frac{\partial^2 h}{\partial y^2}\right)$ are both normal (s_n) and shear (s_s) components, and h is the SLA. It's observed that in regions where relative vorticity predominates, the Okubo-Weiss parameter tends to be negative ($W < 0$). Conversely, in areas where vortex movements within the currents are less pronounced, the Okubo-Weiss parameter tends to be positive ($W > 0$). The Okubo-Weiss parameter is a valuable tool for identifying regions where the shear and normal components of flow exceed the relative vorticity values. When this parameter is negative, it indicates that particle rotation dominates in the fluid. Conversely, when it is positive, it suggests that shear and normal stress components are dominant. Importantly, the Okubo-Weiss parameter can be negative for both cyclones and anticyclones, signifying its utility in characterizing a range of oceanic phenomena.

It's important to emphasize that Figures 6c and 6d illustrate the absence of stretching in the area where the core of the Lofoten anticyclone is located. High vortex activity is observed in the Lofoten basin, while a wide variety of vortex core shapes is observed — from almost round to strongly elongated horizontally or writhing filaments [33, 34, 40, 42, 7, 50, 61]. The main feature of the Lofoten basin is the quasi-permanent anticyclonic Lofoten vortex, which is depicted as a localized formation with limited deformations. Based on this observation, we assume that submesoscale vortices located in the brown-shaded zones should exhibit similar behavior. Therefore, we conclude that unlimited stretching of small vortices is permitted in the vicinity of the core, within a region approximately equivalent to the diameter of the vortex's core. In this region, vortices have the potential to transform into filaments.

When we compare Fig. 6, *a* and 6b with 6c and 6d, a clear pattern emerges. The brown regions in Fig. 6c and 6d predominantly align with the areas occupied by large-scale vortex structures. In Fig. 6a, we can observe two distinct vortices, one being an anticyclone and the other a cyclone. The center of the anticyclone, which is shown in blue in Fig. 6a (negative relative vorticity) has coordinates 69.7° N, 3° E, and the center of the cyclone, which is shown in red in Figure 6a (positive relative vorticity) has coordinates 70.3° N, 4.8° E. It is noteworthy that the cyclone and anticy-

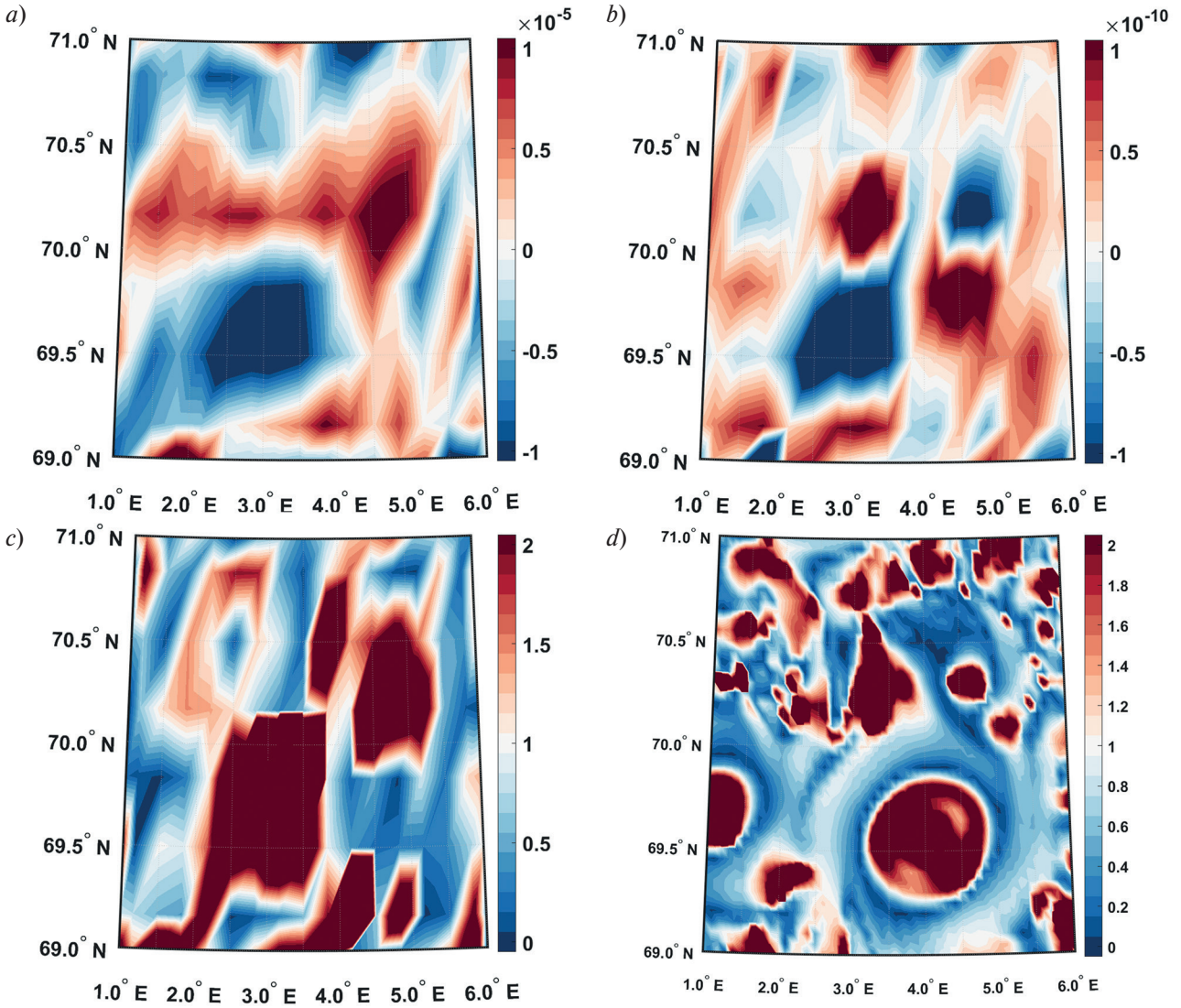

Fig. 6. The spatial distribution of various characteristics in the Lofoten Basin area on June 10, 2010, is depicted as follows: *a* — the relative vorticity; *b* — the Okubo-Weiss parameter; *c* — the parameter $\left|\frac{\gamma}{e}\right|$ according to altimetry; *d* — the parameter $\left|\frac{\gamma}{e}\right|$ according to MIT data. Brown color in *c*) and *d*) indicates areas, where stretching of vortices is prohibited, while blue color corresponds to zones where vortices can be stretched

clone regions show the areas in Figure 6c where stretching is vortex-prohibited. Remarkably, these vortices are also prominently indicated in the Okubo-Weiss parameter field (Fig. 6b). The differences in the location of the regions in Figures 6a and 6b are also understandable since the relative vorticity and the Okubo-Weiss parameter are calculated using different formulas based on data with a spatial resolution of 0.25°. Additionally, let's take into account the important fact that second-order differential derivatives are calculated to construct the distributions for ζ and W.

The differences in Fig. 6c and 6d are determined by the fact that they are based on different datasets. Fig. 6c is based on altimetric data with a spatial resolution of 0.25°, and Fig. 6d is based on data from a high-resolution hydrodynamic model MIT with a spatial resolution of 4 km. It would be very naive to expect a 100 % coincidence of the patterns in the figures constructed using different datasets. On the whole, Fig. 6 reinforces the notion that these large-scale vortices are unable to undergo stretching, as implied by brown-shaded areas in the parameter map (Fig. 6c and 6d). In other words, these stable vortexes are located in the areas where it is a prohibited vortex stretching.

In addition, there are natural limitations due to the framework of the basic theory. Recall that the theory describes barotropic flows with baroclinic vortices, which we approximate by ellipsoids. Of course, this is to a certain extent a first approximation. In the real ocean, things are much more complicated.

A fascinating new characteristic of the World Ocean's eddies has been uncovered. It appears that, under the influence of the deforming effects of large-scale currents, certain mesoscale eddies are undergoing stretching, transforming into filaments. This investigation was conducted using GLORYS12V1 reanalysis data at a spatial resolution of 1/12°, as documented in [5, 6, 31, 32]. However, it has been discovered that this property also applies to altimetric data with a spatial resolution of 0.25°, showcasing the universality of this phenomenon across different datasets and resolutions.

As previously established, there is a notable and consistent preservation of the ratio (approximately 60 %) between the total areas where the stretching of vortices into filaments is allowed and the areas where such stretching is prohibited within the ocean. It is noteworthy that the integrated area of regions where vortices can stretch into filaments predominates over other areas. This ratio remains consistent not only for the entire World Ocean but also for specific oceanic regions, highlighting its universality across different scales of observation.

As vortices undergo stretching, the initial energy concentrated within their characteristic horizontal dimensions is redistributed to smaller scales, roughly aligning with the horizontal width of the resulting filaments. This mechanism represents one of the possible pathways for energy transfer from mesoscale formations to submesoscale motions. This process can be seen as an example of how a portion of energy transitions from the mesoscale to the submesoscale. This mechanism may be considered as the primary method of energy transfer between these scales, illustrating how energy is effectively transferred from larger eddies to smaller-scale features in the ocean.

If we consider a collection of mesoscale eddies in the presence of a large-scale background flow as a geophysical quasi-two-dimensional turbulence, such a system can also undergo a reverse energy redistribution process. In this process, energy transfers from smaller scales to larger ones due to the merging of eddies. However, it's essential to note that merging occurs primarily when vortices are closely spaced. In the context of two-dimensional fluid dynamics, the critical distance between the nearest boundary points of flat vortices is approximately 0.6 times the initial vortex scale, as described in [62]. Nevertheless, it's important to recognize that two-dimensional hydrodynamics offers only a simplified representation of the actual behavior of ocean eddies, and the real dynamics can be more complex and three-dimensional. In the context of three-dimensional hydrodynamics in the ocean, especially for thin eddies (which make up the majority of baroclinic eddies in the ocean), the estimated critical distance for merging is relatively small. In such cases, the merging process requires vortices to come very close to each other, almost making physical contact, as detailed in [18]. This indicates that the dynamics of eddy merging in the ocean can be quite intricate and may differ significantly from the simplified scenarios presented in two-dimensional fluid dynamics.

The process of vortices merging occurs quite rapidly. Therefore, within a collection of eddies, it's expected that closely positioned individual eddies will merge early in their development. Over time, the remaining localized vortices will interact with each other in a manner that resembles their behavior as point vortices. This interaction with the background flow primarily affects the vortices and can result in a significant portion of them stretching into filaments.

During the initial phase of the evolution of an ensemble of vortices in the presence of a deforming flow, it's reasonable to anticipate energy transfer from vortices to filaments. However, the specific mechanisms of vortex energy transfer across the spectrum of scales remain somewhat unclear. Nevertheless, based on the authors' observations, the process of vortices transforming into filaments seems to dominate over the process of vortices merging. This ultimately leads to a comprehensive redistribution of vortex energy from the mesoscale to the submesoscale in the oceanic dynamics.

The assessment of vortex energy has revealed an interesting pattern: as a vortex extends in length, its energy levels, including kinetic energy, available potential energy, and the combined energy of both types, decrease concurrently with the stretching of the vortex core. Theoretical calculations have indicated a substantial decrease in vortex energy when the core undergoes significant elongation, ranging from 20 % to 60 %. These same investigations were applied to the study of real eddies in the Lofoten Basin (as detailed in [24]), where both qualitative and quantitative alignment with theoretical findings was demonstrated.

This raises a natural question: where does the energy lost during the elongation of the vortex go?

Considering that our physical system consists solely of a vortex and a flow, it's reasonable to expect that the vortex's energy will be redistributed to the flow. In the context of an ensemble of eddies as a form of geophysical turbulence, where eddies arise from a flow and subsequently engage in energetic interactions with it, the phenomenon of energy being returned from turbulence to the flow is known as negative viscosity. This phenomenon is highly intriguing and not yet fully understood. Interest in negative viscosity has grown since Victor Starr's publication [29].

In the context of the research, it can be asserted that you have encountered the phenomenon of negative viscosity, and you are even able to identify areas on the map of the World Ocean where this negative viscosity is expected to manifest itself. This suggests that the study contributes to a deeper understanding of the complex dynamics of energy transfer and redistribution within the oceanic system.

These areas can be characterized as domains with the property $\left|\frac{\gamma}{e}\right| \le 1$. All these zones are depicted in blue color in Fig. 3–5, where the combined area of the identified negative viscosity zones is extensive, encompassing approximately 60–66 % of the total area of the World Ocean. However, it should be noted that many physical processes unresolved by $\left|\frac{\gamma}{e}\right|$ maps also can contribute to the sign of viscosity (e. g. instability of the mixed layer, frontal instability, vortex instability, vortex interactions, etc.).

In our work, we neglected the interaction of vortices with vortices, leaving only the interaction of vortices with background currents. Let's try to understand at a qualitative level what new things should turn out if we take into account this interaction. The following happens in the ensemble of interacting vortices. Closely spaced vortices of the same name will merge, and weak vortices will stretch out into filaments. Larger vortex centers surrounded by vortex filaments will appear in the considered ensemble. According to our theory, the size of vortices does not play any role in the ability of vortices to stretch in background flows. Only the potential vorticity of the liquid in the core is important. The background flow, acting on such an altered vortex field, will also pull part of the large vortex centers into filaments. As a result, there will be more vortex filaments than in the case of a simple effect of flows on vortices. The purpose of our work is to show that the conditions for the formation of filaments from vortices are formed in the ocean. Taking into account the interaction of vortices with each other, these conditions will only intensify.

APPENDIX I

In the barotropic ocean, the term potential vorticity is used in the law of conservation of magnitude $\frac{f + rot_z\vec{u}}{H}$, where H is the thickness of a homogeneous liquid layer. For a barotropic background flow $rot_z\vec{u} = 2\gamma$. Here you really need to consider ($f + 2\gamma$). However, in our problem we consider a baroclinic ocean and baroclinic vortices, but with a barotropic background flow. The potential vorticity in our case is different: $\sigma = rot_z\vec{u} + \frac{\partial}{\partial z}\frac{f^2}{N^2}\frac{\partial \psi}{\partial z}$ (ψ is the current function) and does not match with $\frac{f + rot_z\vec{u}}{H}$ neither in physics nor in dimension. Therefore, it is not necessary to add f and $rot_z\vec{u}$ in this study.

APPENDIX II

To analyze the behavior of vortices in the flow (1), we apply the theory of dimension. In the background flow $\vec{u} = (u, v, 0)$, the coefficients e and γ have the same dimension m^{-1}. An ellipsoidal vortex, in addition to three geometric dimensions — the lengths of the semi–axes, has another dimensional parameter σ which means excess of the potential vorticity of the core over the potential vorticity of the background flow. The potential vorticity of the barotropic background flow σ coincides with the relative vorticity $\gamma = \frac{1}{2} rot_z\vec{u}_b(x, y)$. The dimensions of σ and the relative vorticity of the background flow also coincide.

Let's return to the geometric parameters of the vortex core. Let us denote the sizes of the horizontal semi-axes of the vortex core as a and b, and the size of the vertical half-axis is c. Note that the problem of the evolution of an ellipsoidal core is studied at a constant the Väisälä-Brunt frequency N [25–28, 18, and references herein). The problem of vortex evolution is formulated in a mathematical space where the vertical z-axis is stretched (N)/f times (f is the Coriolis parameter). As a result, in such a vertically stretched space, the horizontal half-axes a and b of the ellipsoid remained the same, and the vertical half-axis stretched (N)/f times. Denote the stretched axis as $\tilde{c} = \frac{N}{f}c$. In barotropic flows (2), the vertical semi-axis $\tilde{c}$ does not change, and the horizontal semi-axis change so that their product $a(t) \times b(t)$ is also preserved. In this formulation, the vortex core has three dimensional geometric parameters a, b and $\tilde{c}$, from which two dimensionless geometric parameters of the vortex can be made, and they are the parameter of horizontal elongation $\varepsilon = a/b$ and the parameter of vertical oblateness of the core $K = \frac{\tilde{c}}{\sqrt{a\,b}}$. The parameter K for each vortex does not change, while ε changes with time. From a set of other dimensional parameters of the problem

e, γ and σ, it is also possible to compose two dimensionless parameters $(\gamma)/e$ and $(\sigma)/e$, which do not change over time for each vortex in its flow. There is another dimensionless parameter in the problem, i. e. the orientation angle of the vortex θ or the angle of rotation for the certainty of the semi-axis of the ellipsoid a with respect to the x-axis of a convenient coordinate system. In this formulation, it is possible to reduce the problem of the behavior of a vortex in a barotropic flow to the problem of the evolution of two variables over time of the vortex parameters ε and θ depending on the remaining dimensionless parameters $(\sigma)/e$, $(\gamma)/e$ and K. In the complete mathematical formulation of the problem, we should add the initial conditions for ε and θ, denote them ε_0 and θ_0.

As a result, the problem of vortex behavior in the flow (2) can be considered on the plane of dimensionless parameters $((\sigma)/e, (\gamma)/e)$ for a set of fixed values of K. Let's choose the most characteristic value of the flatness parameter $K = 0.2$. Of course, other values of K may also occur, so additionally consider $K = 0.1$ and $K = 0.3$. When the parameter K is changed, the boundaries separating zones with different behavior of vortices in the band $|(\gamma)/e|<1$ change. Decreasing the parameter K will expand the boundaries of the purple zone in Figure 2. Options for changing the boundaries of zones of different vortex behavior at different values of K are shown in Figure A1. The coefficient of boundary expansion (or the coefficient of boundary recalculation for other values of K) is proposed in Figure A2. The same conversion factor is valid for the boundaries between the yellow and purple zones. Thus, the boundaries in Figure 2 are self-similar, i. e. they are obtained from each other by stretching or compressing the scale of the horizontal axis $(\sigma)/e$. From $K = 0.2$, we can obtain these boundaries for other values of K.

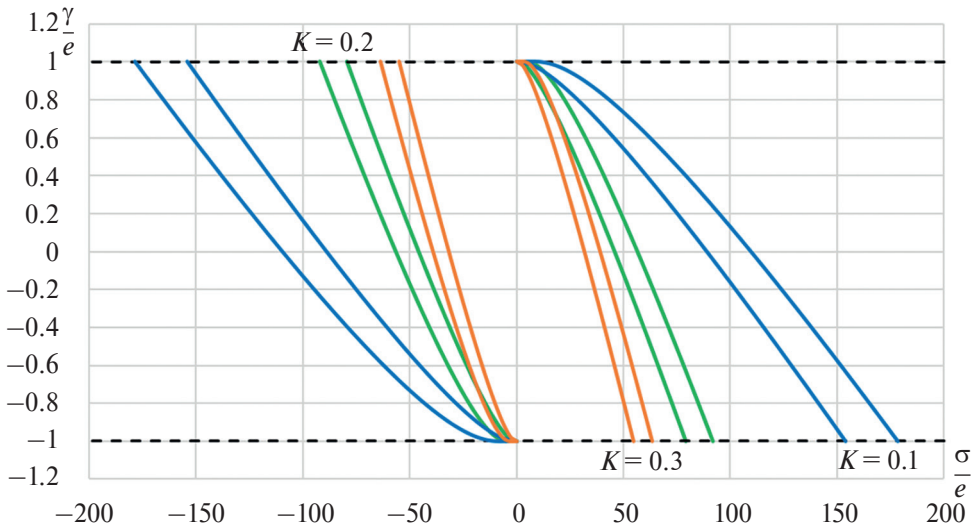

Fig. A1. The nature of the change in the boundaries of zones of different behavior of vortices at different values $K = 0.1, 0.2, 0.3$ in the plane of dimensionless characteristics $((\sigma)/e, (\gamma)/e)$

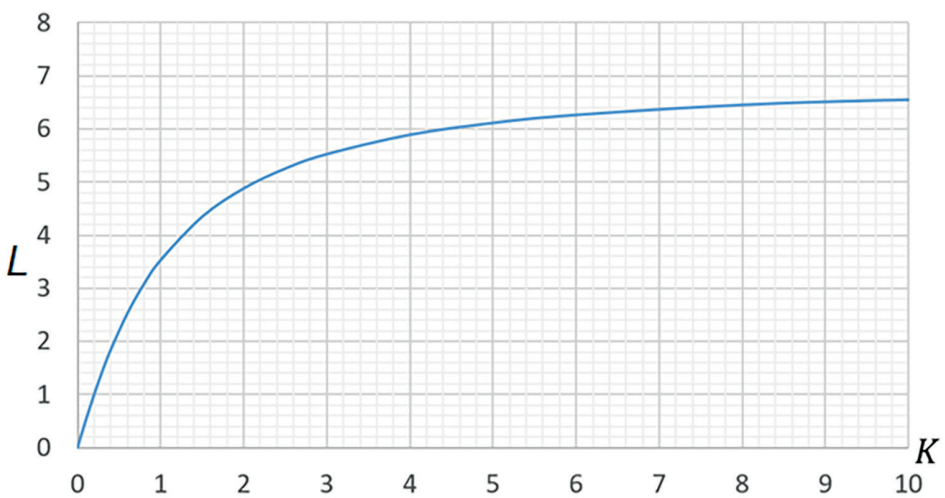

Fig. A2. The scaling factor L of the boundaries of the regions of different behavior of vortices

APPENDIX III

The famous scientist Kirchhoff [63] mathematically formulated and solved the problem of the behavior of a vortex in the form of an elliptical equal-vortex region in a medium at rest at infinity for the case of an ideal fluid. Such a vortex is called a Kirchhoff vortex and is an exact solution of the Euler equations for the case of plane hydrodynamics of an ideal fluid. According to Kirchhoff, the behavior of an elliptical equal-vortex region was reduced to the rotation of the ellipse (rotation of the shape of the vortex core) with a constant angular velocity without changing the lengths of the ellipse axes. The fluid particles inside the elliptical vortex core overtake the rotation of the shape. The center of the vortex stands still. All hydrophysical fields are continuous. In particular, the velocity field is continuous, but the derivatives of the tangential velocity normal to the vortex boundary break at the boundary itself, therefore the vorticity changes abruptly, which is included in the formulation of the problem. The speed inside the ellipse increases from the center to the boundary of the ellipse, and it decreases outside the ellipse with asymptotic behavior $1/R$ at large distances R. The next generation of researchers solved the problem of the evolution of the Kirchhoff vortex in background flows.

The next generation of researchers solved the problem of the evolution of the Kirchhoff vortex in background flows. The Japanese hydrodynamicist Kida [15], who described the behavior of the Kirchhoff vortex in equally vortex flows of plane hydrodynamics, coped with this problem most successfully. Equally swirling flows were not chosen by Kida by chance. Only in such flows will the vortex, being elliptical at the initial moment, remain elliptical further. But at the same time, the elliptical vortex core moves as a whole along the flow at the speed of the background flow at the center of the vortex. In this case, the core can rotate, and deform with rotating, remaining an ellipse. Kid's work gave rise to a huge number of theoretical, laboratory, and numerical studies on the evolution of Kirchhoff vortices in the flows.

Let's take a closer look at the background currents that Kida used. These are flat incompressible flows with velocities linearly dependent on coordinates

$$\begin{aligned} u &= u_0 + e\,x - \gamma_1 y, \\ v &= v_0 + \gamma_2 x - e\,y. \end{aligned} \tag{A1}$$

Здесь (x, y) — произвольная система ортогональных координаты; u_0, v_0, e, γ_1, γ_2 константы, привязанные к выбранной системе координат. При изменении системы координат, например, при повороте, все указанные константы u_0, v_0, e, γ_1, γ_2.

Here (x, y) is an arbitrary system of orthogonal coordinates; u_0, v_0, e, γ_1, γ_2, are the constants tied to the selected coordinate system. When changing the coordinate system, for example, when rotating, all specified constants u_0, v_0, e, γ_1, γ_2 will change. However, a number of properties should be preserved. For example, the linear dependence (A1) on coordinates will be preserved in any coordinate system. Further, in any system, the coefficient e for x in the first equation and the coefficient e for y in the second equation must be identical in magnitude but have different signs. However, the coefficient e will change when changing the coordinate system. Finally, it follows from the equality $\gamma_1 + \gamma_2 = \dfrac{\partial v}{\partial x} - \dfrac{\partial u}{\partial y}$ that the sum of the coefficients $g_1 + g_2$ is the same in any coordinate system. Further, by a parallel shift, you can always select a coordinate system in which $u_0 = v_0 = 0$. In this coordinate system:

$$\begin{cases} u = ex - \gamma_1 y \\ v = \gamma_2 x - ey. \end{cases} \tag{A2}$$

Let's consider two coordinate systems: the old (x, y) and a new $(\tilde{x}, \tilde{y})$. In the new coordinate system, the property of linearity will be preserved:

$$\begin{cases} \tilde{u} = \tilde{e}\tilde{x} - \tilde{\gamma}_1 \tilde{y} \\ \tilde{v} = \tilde{\gamma}_2 \tilde{x} - \tilde{e}\widetilde{y}. \end{cases} \tag{A3}$$

Naturally, e and $\tilde{e}$ differ from each other, but $\gamma_1 + \gamma_2 = 2\tilde{\gamma} = rot_z \vec{u}$. Let the new system be turned to the old one at an angle α. Then the coefficients e, γ_1, γ_2 and $\tilde{e}$, $\tilde{\gamma}_1, \tilde{\gamma}_2$ are related by the relations

$$\tilde{e}_1 = e_1 \cos 2\alpha - \frac{1}{2}(\gamma_1 - \gamma_2)\sin 2\alpha\,,$$

$$\tilde{\gamma}_1 = e_1 \sin 2\alpha + \frac{1}{2}(\gamma_1 + \gamma_2) + \frac{1}{2}(\gamma_1 - \gamma_2)\cos 2\alpha, \tag{A4}$$

$$\tilde{\gamma}_2 = -e_1 \sin 2\alpha + \frac{1}{2}(\gamma_1 + \gamma_2) - \frac{1}{2}(\gamma_1 - \gamma_2)\cos 2\alpha$$

Statement: you can always choose such a coordinate system (find the angle of rotation α), wherein $\tilde{\gamma}_1 = \tilde{\gamma}_2 = \tilde{\gamma}$. In this case

$$e_1 \sin 2\alpha + \frac{1}{2}(\gamma_1 + \gamma_2) + \frac{1}{2}(\gamma_1 - \gamma_2)\cos 2\alpha = -e_1 \sin 2\alpha + \frac{1}{2}(\gamma_1 + \gamma_2) - \frac{1}{2}(\gamma_1 - \gamma_2)\cos 2\alpha,$$

$$e_1 \sin 2\alpha + \frac{1}{2}(\gamma_1 - \gamma_2)\cos 2\alpha = 0,$$

$$\mathrm{tg}2\alpha = -\frac{\gamma_1 - \gamma_2}{2e_1}.$$

In the new coordinate system

$$\tilde{\gamma}_1 = \tilde{\gamma}_2 = \tilde{\gamma} = \frac{1}{2}(\gamma_1 + \gamma_2),$$

$$\tilde{e}_1 = \sqrt{e_1^2 + \frac{1}{4}(\gamma_1 - \gamma_2)^2}.$$

For uniformity, we denote $\tilde{e} = \tilde{e}_1$. Thus, with a linear dependence of the speed of flat currents on coordinates, it is always possible to select a coordinate system in which the speed field looks like this:

$$\begin{aligned} u &= \tilde{e}x - \tilde{\gamma}y \\ v &= \tilde{\gamma}x - \tilde{e}y \end{aligned}.$$

Now let us explain why, following Kida, we consider such a coordinate system convenient. The point is this. If we worked with the old coordinate system, in which the velocity field would be given by relations (A2), then the equations for the evolution of the parameters of an elliptical vortex look as follows

$$\dot{a} = -b\left[e\cos 2\theta - \frac{1}{2}(\gamma_1 - \gamma_2)\sin 2\theta \right],$$

$$\dot{b} = a\left[e\cos 2\theta - \frac{1}{2}(\gamma_1 - \gamma_2)\sin 2\theta \right],$$

$$\dot{\theta} = \Omega(a,b) + \frac{1}{2}(\gamma_1 + \gamma_2) - \frac{a^2 + b^2}{a^2 - b^2}\left[e\sin 2\theta + \frac{1}{2}(\gamma_1 - \gamma_2)\cos 2\theta \right].$$

Here a and b are the values of the horizontal semi-axes of the ellipse and θ is the orientation angle of the vortex core in this coordinate system (the angle between axis a and the positive direction of axis x). $\Omega(a, b)$ is the own angular velocity of rotation of the ellipse in the absence of external flow:

$$\Omega(a,b) = \sigma\frac{\varepsilon}{(\varepsilon+1)^2}, \qquad \varepsilon = \frac{a}{b}.$$

Here σ is the excess of the vortex core vorticity over the vorticity of the external flow. Note that the deformation of the semi-axes of the ellipse a and b in this coordinate system depends on all parameters of the external flow e, γ_1, γ_2.

If we move to a convenient coordinate system proposed by Kida, then the same velocity field in it is presented as

$$\begin{aligned} \tilde{u} &= \tilde{e}\tilde{x} - \tilde{\gamma}\tilde{y} \\ \tilde{v} &= \tilde{\gamma}\tilde{x} - \tilde{e}\tilde{y} \end{aligned},$$

and the evolution equations for the same vortex for a, b, and orientation angle θ look much simpler:

$$\dot{a} = -b\tilde{e}\cos 2\tilde{\theta},$$

$$\dot{b} = a\tilde{e}\cos 2\tilde{\theta},$$

$$\dot{\theta} = \Omega(a,b) + \tilde{\gamma} - \frac{a^2 + b^2}{a^2 - b^2}\tilde{e}\sin 2\tilde{\theta}.$$

Here $\tilde{\theta}$ is the angle of orientation of the vortex in the new coordinate system.

When described in a convenient Kida's coordinate system, only one parameter $\tilde{e}$ of the external flow is responsible for the vortex deformation, calculated in the above convenient coordinate system. That is why $\tilde{e}$ is called the deformation coefficient. In the general case, the coordinate system, which is convenient for studying the behavior of elliptical vortices in external flows, differs from the standard coordinate system for geophysicists, where the *x*-axis is directed to the East. To understand how vortices behave in the flows, we need to know only two flow parameters from a convenient coordinate system: the deformation coefficient $\tilde{e}$ and the vertical component of the background flow vorticity $\tilde{\gamma} = \frac{1}{2} rot_z \vec{u}$, which generally does not depend on the choice of the coordinate system. Therefore, the only parameter we need from a convenient coordinate system is the deformation coefficient $\tilde{e}$.

An equally swirling horizontal flow, independent of the vertical coordinate, has its name in oceanology — barotropic flow. When studying three-dimensional ellipsoidal vortices in barotropic flows, a convenient coordinate system coincides with Kida's coordinate system, and the behavior of the vortex characteristics differs only in the form of the function $\Omega(a, b)$, which in the case of ellipsoidal vortices will be more complex and will additionally depend on the size of the vertical semi-axis *c*.

Let's return to the flow field in the convenient Kida's coordinate system:

$$\begin{aligned} \tilde{u} &= \tilde{e}\tilde{x} - \tilde{\gamma}\tilde{y} \\ \tilde{v} &= \tilde{\gamma}\tilde{x} - \tilde{e}\tilde{y} \end{aligned}.$$

Further, we will work only in this coordinate system, so to simplify the recording we will discard the "tilde" sign on all letters

$$\begin{cases} u = ex - \gamma y \\ v = \gamma x - ey \end{cases}.$$

Moving on to the stream function $\psi(a, b)$, we get $u = \frac{\partial \psi}{\partial y}$ $v = -\frac{\partial \psi}{\partial x}$, and

$$\begin{aligned} \frac{\partial \psi}{\partial y} &= ex - \gamma y \\ \frac{\partial \psi}{\partial x} &= -\gamma x + ey \end{aligned}.$$

The solution to this system of equations

$$\psi(x, y) = -\frac{1}{2}\gamma\left(x^2 + y^2\right) + exy + C,$$

where *C* is the integration constant. Stream function isolines $\psi(x, y) = \text{const}$ in the stationary case coincide with the trajectories of particles. Therefore, the set of lines

$$-\frac{1}{2}\gamma\left(x^2 + y^2\right) + exy = \text{const}$$

represents a set of trajectories of particles of equally swirling flows. Flows with different values *e* and γ describe completely the entire variety of equally swirling barotropic flows. The quadratic dependence of the trajectory equations indicates that the trajectories of motion can be hyperbolas and ellipses and, in the frequent case, plane-parallel flow with a constant velocity shift. An ellipsoidal vortex placed in an equally swirling barotropic flow will move as a whole with the speed of the background flow at its center. Simultaneously with the movement of the vortex as a whole, the vortex is subjected to the deforming influence of the background flow, so vortices in the flows with $\left|\frac{\gamma}{e}\right| \le 1$ can stretch out. The inequality $|\gamma/e| > 1$ is a necessary condition for prohibiting the stretching of vortices. Everything that has been said is presented in detail, starting from [63] for two-dimensional hydrodynamics and also [5, 21, 22, 18].

Funding

Theoretical aspects of this research were developed under the auspices of the Institute of Oceanology of the Russian Academy of Sciences (State Assignment No. FMWE-2024-0016). Computational work was supported by St. Petersburg University (Grant No. 116442164). Figure generation and analysis of vortex evolution were supported by the Russian Science Foundation (Grant No. 24-77-00063; https://rscf.ru/project/24-77-00063/).

References

1. Chelton D.B., Schlax M.G., Samelson R.M. Global observations of nonlinear mesoscale eddies. *Progress in Oceanography*. 2011;91:167–216. doi:10.1016/j.pocean.2011.01.002
2. Wood R.A. Mesoscale/Synoptic Coherent structures in Geophysical Turbulence. Editors: B.M. Jamart, J.C.J. Nihoul. 1989;50:265, 9780444874702
3. Nencioli F., Dong C., Dickey T.D., Washburn L., McWilliams J.C. A vector geometry based eddy detection algorithm and its application to a high-resolution numerical model product and high-frequency radar surface velocities in the Southern California Bight. *Journal of Atmospheric and Oceanic Technology*. 2010;27(3):564–579. doi:10.1175/2009jtecho725.1
4. Gurova E.S., Ivanov A. Yu. Appearance of Sea Surface Signatures and Current Features in the South-East Baltic Sea on the MODIS and SAR images. *Sovremennye Problemy Distantsionnogo Zondirovaniya Zemli iz Kosmosa*. 2011;4:41–54 (In Russ.).
5. Zhmur V.V., Belonenko T.V., Novoselova E.V., Suetin B.P. Conditions for Transformation of a Mesoscale Vortex into a Submesoscale Vortex Filament When the Vortex Is Stretched by an Inhomogeneous Barotropic Flow. *Oceanology*. 2023;63(2):174–183. doi:10.1134/S0001437023020145
6. Zhmur V.V., Belonenko T.V., Travkin V.S. et al. Changes in the Available Potential and Kinetic Energy of Mesoscale Vortices When They Are Stretched into Filaments. *Journal of Marine Science and Engineering*. 2023;11:1131. doi:10.3390/jmse11061131
7. Belonenko T.V., Zinchenko V.A., Fedorov A.M. et al. Interaction of the Lofoten Vortex with a satellite cyclone. *Pure and Applied Geophysics*. 2021;178:287–300. doi:10.1007/s00024-020-02647-1
8. Batchelor G.K. An Introduction to Fluid Dynamics. Cambridge at the University Press; 1970. 778 p.
9. McDowell S.E., Rossby H.T. Mediterranean Water: An Intense Mesoscale Eddy off the Bahamas. *Science*. 1978;202(4372): 1085–1087. doi:10.1126/science.202.4372.1085
10. Carton X. Hydrodynamical Modeling Of Oceanic Vortices. *Surveys in Geophysics*. 2001;22:179–263. doi:10.1023/A:1013779219578
11. Fer I., Bosse A., Ferron B., Bouruet-Aubertot P. The dissipation of kinetic energy in the Lofoten Basin Eddy. *The Journal of Physical Oceanography*. 2018;48(6):1299–1316. doi:10.1175/JPO-D-17–0244.1
12. Zhmur V.V., Novoselova E.V., Belonenko T.V. Peculiarities of Formation the of Density Field in Mesoscale Eddies of the Lofoten Basin: Part 2. *Oceanology*. 2022;62(3):289–302. doi:10.1134/S0001437022030171
13. Chaplygin S.A. On a pulsating cylindrical vortex. *Trans. Phys. Sect. Imperial Moscow Soc. Friends of Natural Sciences*. 1899;10(1):13–22.
14. Chaplygin S.A. Collected Works, Vol. 2. Moscow, Leningrad: Gostekhizdat; 1948:643 p. (in Russ.).
15. Kida S. Motion of an Elliptic Vortex in a Uniform Shear Flow. *Journal of the Physical Society of Japan*. 1981;50(10):3517–3520. doi:10.1143/JPSJ.50.3517
16. Polvani L.M., Flierl G.R. Generalized Kirchhoff vortices. *Physics Fluids*. 1986;29:2376–2379. doi:10.1063/1.865530
17. McKiver W.J., Dritschel G.G. Balanced solutions for an ellipsoidal vortex in a rotating stratified flow. *Journal of Fluid Mechanics*. 2016;802:333–358. doi:10.1017/jfm.2016.462
18. Zhmur V.V. *Mesoscale Ocean Eddies*. Moscow: GEOS; 2011. 289 p. (in Russ.).
19. Zhmur V.V., Novoselova E.V., Belonenko T.V. Peculiarities of formation of the density field in mesoscale eddies of the Lofoten Basin: Part 1. *Oceanology*. 2021;61(6):830–838. doi:10.1134/S0001437021060333
20. Zhmur V.V., Novoselova E.V., Belonenko T.V. Potential Vorticity in the Ocean: Ertel and Rossby Approaches with Estimates for the Lofoten Vortex. *Izvestiya, Atmospheric and Oceanic Physics*. 2021;57(6):632–641. doi:10.1134/S0001433821050157
21. Meacham S.P. Quasigeostrophical ellipsoidal vortices in stratified fluid. *Dynamics of Atmospheres and Oceans*. 1992;16(3–4):189–223.
22. Meacham S.P., Pankratov K.K., Shchepetkin A.F., Zhmur V.V. The interaction of ellipsoidal vortices with background shear flows in a stratified fluid. *Dynamics of Atmospheres and Oceans*. 1994;21(2–3):167–212. doi:10.1016/0377-0265(94)90008-6
23. Zhmur V.V., Harutyunyan D.A. Redistribution of Energy during Horizontal Stretching of Ocean Vortices by Barotropic Currents. *Oceanology*. 2023;63:1–16. doi: P10.1134/S0001437023010186
24. Zhmur V.V., Travkin V.S., Belonenko T.V., Arutyunyan D.A. Transformation of Kinetic and Potential Energy during Elongation of a Mesoscale Vortex. *Physical Oceanography*. 2022;29(5):449–462. doi:10.22449/1573-160X-2022-5-449-462
25. McKiver W.J., Dritschel D.G. The motion of a fluid ellipsoid in a general linear background flow. *Journal of Fluid Mechanics*. 2003;474:147–173. doi:10.1017/S0022112002002859
26. McKiver W.J., Dritschel D.G. The stability of a quasi-geostrophic ellipsoidal vortex in a background shear flow. *Journal of Fluid Mechanics*. 2006;560:1–17. doi:10.1017/S0022112006000462

27. Dritschel D.G., Reinaud J.N., McKiver W.J. The quasi-geostrophic ellipsoidal vortex model. *Journal of Fluid Mechanics*. 2004;505:201–223. doi:10.1017/s0022112004008377
28. Reinaud J.N., Dritschel D.G. The merger of vertically offset quasi-geostrophic vortices, *Journal of Fluid Mechanics*. 2002;469:287–315. doi:10.1017/s0022112002001854
29. Starr V.P. Physics of Negative Viscosity Phenomena. *McGraw-Hill*. 1968; 256 p.
30. Volkov D.L., Belonenko T.V., Foux V.R. Puzzling over the dynamics of the Lofoten Basin — a sub-Arctic hot spot of ocean variability. *Geophysical Research Letters*. 2013; 40(4):738–743. doi:10.1002/grl.50126
31. Zhmur V.V., Belonenko T.V., Novoselova E.V., Suetin B.P. Direct and Inverse Energy Cascades in the Ocean during Vortex Elongation. *Doklady Earth Sciences*. 2023;508(2): 233–236. doi:10.1134/S1028334X22601675
32. Zhmur V.V., Belonenko T.V., Novoselova E.V., Suetin B.P. Application to the World Ocean of the Theory of Transformation of a Mesoscale Vortex into a Submesoscale Vortex Filament When the Vortex Is Elongated by an Inhomogeneous Barotropic Flow. *Oceanology*. 2023;63(2):184–194. doi:10.1134/S0001437023020157
33. Zinchenko V.A., Gordeeva S.M., Sobko Yu.V., Belonenko T.V. Analysis of Mesoscale eddies in the Lofoten Basin based on satellite altimetry. *Fundamental and Applied Hydrophysics*. 2019;12(3):46–54. doi:10.7868/S2073667319030067
34. Fedorov A.M., Belonenko T.V. Interaction of mesoscale vortices in the Lofoten Basin based on the GLORYS database. *Russian Journal of Earth Sciences*. 2020;20: ES2002. doi:10.2205/2020ES000694
35. Raj R.P., Halo I., Chatterjee S., Belonenko T., Bakhoday-Paskyabi M., Bashmachnikov I., Fedorov A., Xie J. Interaction between mesoscale eddies and the gyre circulation in the Lofoten Basin. *Journal of Geophysical Research*: *Oceans*. 2020;125(7): e2020JC016102. doi:10.1029/2020JC016102
36. Le Traon P.Y., Reppucci A., Alvarez Fanjul E., et al. From observation to information and users: The Copernicus Marine Service perspective. *Frontiers in Marine Science*. 2019;6: 234. doi:10.3389/fmars.2019.00234
37. Pujol M.-I., Faugère Y., Taburet G., Dupuy S., Pelloquin C., Ablain M., Picot N. DUACS DT2014: the new multi-mission altimeter data set reprocessed over 20years. *Ocean Science*. 2016;12(5):1067–1090. doi:10.5194/os-12-1067-2016
38. Volkov D.L., Kubryakov A., Lumpkin R. Formation and variability of the Lofoten Basin vortex in a high-resolution ocean model. *Deep Sea Research*. Part I. 2015;105:142–157. doi:10.1016/j.dsr.2015.09.001
39. Gaube P., McGillicuddy Jr.D.J., Moulin A.J. Mesoscale eddies modulate mixed layer depth globally. *Geophysical Research Letters*. 2019;46:1505–1512. doi: 10.1029/2018GL080006
40. Gordeeva S., Zinchenko V., Koldunov A., Raj R.P., Belonenko T. Statistical analysis of long-lived mesoscale eddies in the Lofoten Basin from satellite altimetry. Advances in Space Research. 2021;68(2):364–377. doi:10.1016/j.asr.2020.05.043
41. Sandalyuk N.V., Belonenko T.V. Three-Dimensional Structure of the mesoscale eddies in the Agulhas Current region from hydrological and altimetry data. *Russian Journal of Earth Sciences*. 2021;21: ES4005. doi:10.2205/2021ES000764
42. Sandalyuk N.V., Bosse A., Belonenko T.V. The 3-D structure of mesoscale eddies in the Lofoten Basin of the Norwegian Sea: A composite analysis from altimetry and in situ data. *Journal of Geophysical Research*: *Oceans*. 2020;125: e2020JC016331
43. Yu L.-S., Bosse A., Fer I., Orvik K.A., Bruvik E.M., Hessevik I., Kvalsund K. The Lofoten Basin eddy: Three years of evolution as observed by Seagliders. *Journal of Geophysical Research*: *Oceans*. 2017;122:6814–6834. doi:10.1002/2017JC012982
44. Rossby T., Ozhigin V., Ivshin V., Bacon S. An isopycnal view of the Nordic seas hydrography with focus on properties of the Lofoten Basin. *Deep Sea Research*. Part I. 2009;56(11):1955–1971. doi:10.1016/j.dsr.2009.07.005
45. Andersson M., LaCasce J.H., Koszalka I., Orvik K.A., Mauritzen C. Variability of the Norwegian Atlantic Current and associated eddy field from surface drifters. *Journal of Geophysical Research*: *Oceans*. 2011;116: C08032. doi:10.1029/2011JC007078
46. Koszalka I., LaCasce J.H., Andersson M.K., Orvik A., Mauritzen C. Surface circulation in the Nordic seas from clustered drifters. *Deep Sea Research*. Part I. 2011;58:468–485. doi:10.1016/j.dsr.2011.01.007
47. Søiland H., Rossby T. On the structure of the Lofoten Basin Eddy. *Journal of Geophysical Research*: *Oceans*. 2013;118:4201–4212. doi:10.1002/jgrc.20301
48. Belonenko T.V., Koldunov A.V., Sentyabov E.V., Karsakov A.L. Thermohaline structure of the Lofoten vortex in the Norwegian Sea based on in-situ and model data. *Vestn. S.-Peterb. Univ., Nauki Zemle*. 2018; 63(4): 502–519. doi:10.21638/spbu07.2018.406
49. Bosse A., Fer I., Søiland H., Rossby T. Atlantic water transformation along its poleward pathway across the Nordic Seas. *Journal of Geophysical Research*: *Oceans*. 2018;123: 6428–6448. doi;10.1029/2018JC014147
50. Travkin V.S., Belonenko T.V. Seasonal variability of mesoscale eddies of the Lofoten Basin using satellite and model data. *Russian Journal of Earth Sciences*. 2019;19: ES5004. doi:10.2205/2019ES000676
51. Raj R.P., Chafik L., Even J., Nilsen O., Eldevik T., Halo I. The Lofoten vortex of the Nordic seas. *Deep Sea Research*. Part I. 2015;96:1–14. doi:10.1016/j.dsr.2014.10.011
52. Raj R.P., Johannessen J.A., Eldevik T., Nilsen J.E.O., Halo I. Quantifying mesoscale eddies in the Lofoten Basin. *Journal of Geophysical Research*. 2016;121:4503–4521. doi:10.1002/2016JC01163.7

53. Köhl A. Generation and stability of a quasi-permanent vortex in the Lofoten Basin. *Journal of Physical Oceanography*. 2007;37(11):2637–2651. doi:10.1175/2007jpo3694.1
54. Belonenko T.V., Volkov D.L., Ozhigin V.K., Norden Yu.E. Water circulation in the Lofoten Basin of the Norwegian Sea. *Vestn. S.-Peterb. Univ., Ser. 7: Geol., Geogr*. 2014;2:108–121 (In Russ.).
55. Bashmachnikov I.L., Belonenko T.V., Kuibin P.A. Application of the theory of columnar Q-vortices with helical structure for the Lofoten vortex in the Norwegian Sea. *Vestn. S.-Peterb. Univ., Nauki Zemle*. 2017;62(3):221–336. doi:10.21638/11701/spbu07.2017.301
56. Bashmachnikov I.L., Fedorov A.M., Vesman A.V., Belonenko T.V., Dukhovskoy D.S.. Thermohaline convection in the subpolar seas of the North Atlantic from satellite and in situ observations. Part 2: Indices of intensity of deep convection. *Sovremennye Problemy Distantsionnogo Zondirovaniya Zemli iz Kosmosa*. 2019;16(1):191–201. doi:10.21046/2070-7401-2019-16-1-191-201
57. Bashmachnikov I.L., Fedorov A.M., Vesman A.V., Belonenko T.V., D.S. Dukhovskoy. Thermohaline convection in the subpolar seas of the North Atlantic from satellite and in situ observations. Part 1: Localization of the deep convection sites. *Sovremennye Problemy Distantsionnogo Zondirovaniya Zemli iz Kosmosa*. 2018;15(7):184–194. doi:10.21046/2070-7401-2018-15-7-184-194
58. Bashmachnikov I.L., Sokolovskiy M.A., Belonenko T.V., Volkov D.L., Isachsen P.E., Carton X. On the vertical structure and stability of the Lofoten Vortex in the Norwegian Sea. *Deep Sea Research*. Part I. 2017;128;1–27. doi:10.1016/j.dsr.2017.08.001
59. Okubo A. Horizontal dispersion of floatable particles in the vicinity of velocity singularities such as convergences. *Deep Sea Research and Oceanographic Abstracts* 1970;17:445–454. doi:10.1016/0011-7471(70)90059-8
60. Weiss J. The dynamics of enstrophy transfer in two dimensional hydrodynamics. *Physica D*. 1991;48(2–3):273–294. doi:10.1016/0167-2789(91)90088-q
61. Travkin V.S., Belonenko T.V., Budyansky M.V., Prants S.V., Uleysky M.Y., Gnevyshev V.G., et al. Quasi-Permanent Mushroom-like Dipole in the Lofoten Basin. *Pure and Applied Geophysics*. 2022;179(1):465–482. doi:10.1007/s00024-021-02922-9
62. Griffiths R.W., Hopfinger E.J. Coalescing of geostrophic vortices. *Journal of Fluid Mechanics*. 1987;178:73–97. doi:10.1017/S0022112087001125
63. Kirchhoff G. Vorlesungen über matematische Physic: Mechanik. Leipzig: Teubner; 1876. 489 p.

About the Authors

ZHMUR, Vladimir V., Head of the Laboratory, Chief Researcher, Dr. Sc. (Phys.-Math.), Corresponding Member of the Russian Academy of Sciences, SPIN-code (РИНЦ): 5553-8019, ORCID: 0000-0001-8217-0932, WoS ResearcherID: P-9738-2015, Scopus AuthorID: 6602162918, e-mail: zhmur-vladimir@mail.ru

BELONENKO, Tatyana V., Professor of the Department of Oceanology at St. Petersburg State University, SPIN-code (РИНЦ): 1978-1620, ORCID: 0000-0003-4608-7781, Scopus Author ID: 6507005889, WoS ResearcherID: K-2162-2013, e-mail: btvlisab@yandex.ru

NOVOSELOVA, Elena V., Researcher at St. Petersburg State University and Nansen International Environmental and Remote Sensing Center Scientific Foundation, SPIN-code (РИНЦ): 3244-7881, ORCID: 0000-0002-6319-8937, WoS ResearcherID: AAZ-6650-2020, Scopus AuthorID: 57219992097, e-mail: novoselovaa.elena@gmail.com

SUETIN, Boris P., Postgraduate student at the Moscow Institute of Physics and Technology (National Research University), Scopus AuthorID: 58153398500, e-mail: suetinboris@gmail.com